International Workshop „Magnetic Resonance Studies“

June 25 - 27, 2012

Oberschwarzenberg, Austria

Book of Abstracts

Supported by
„Aktion Austria - Czech Republic“
63p18

Monday, June 25, 2012

13:15 Welcome -introduction

13:30-15:30 Scientific session 1

IMCL measurement by combined FID and echo acquisition
I Just Kukurová, W. Bogner, L. Valkovič, M. Gajdošík, M. Bittsansky, M. Krššák, S. Gruber, S.Trattnig, M. Chmelik.

^{1}H MR Relaxation Times of Lipid Compounds in Liver at 7.0 T
M. Gajdošík, M. Chmelík, W. Bogner, I. Just Kukurová, S. Trattnig, M. Krššák

In-vivo chemical shift imaging of the human brain spectroscopy at 9.4 T – preliminary results
G.L. Chadzynski, S. Gunamony, R. Kolb, R. Pohmann, U. Klose, K. Scheffler

Increasing the SNR in MRSI by Combining the Channels of an Array Coil Using GRE Images for Phasing
B. Strasser, M. Chmelik, S. Trattnig, S. Gruber, W. Bogner

Pulse cascaded Hadamard Spectroscopic Imaging with short acquisition delay in the brain at 7T
G. Hangel, W. Bogner

B1+ mapping of ^{31}P coils by steady state CSI
M. Chmelík, L. Valkovič, M. Považan, I. Just Kukurová, S. Gruber, M. Krššák, S. Trattnig, W. Bogner

2D CSI simultanous FID and long echo time acquisition of IMCL at 7T

I. Just Kukurová}[1, 2], W. Bogner[1], L. Valkovič[1], M. Gajdošík[1], M. Bittsansky[3], M. Kršňák[1], S. Gruber[1], S. Trattnig[1], M. Chmelik[1];
[1]Vienna/AT, [2]Bratislava/SK, [3]Martin/SK

Purpose / Introduction
Analysis of intramyocellular lipids (IMCL) in skeletal muscle is demanding task especially because of the spectral overlap with extramyocellular lipids (EMCL) shifted by~0.2ppm [1]. Short echo time spectroscopy with water suppression (WS) and outer volume suppression (OVS) provide high SNR but strong spectral overlaps [1-3]. On the other hand long echo time spectroscopy was suggested for simplifying spectra [4-5]. In this study we introduce sequence for CSI with simultanous FID and long echo time acquisition in one measurement at 7T. Sequence should provide efficient subcutaneous lipid suppression through improved PSF function (high matrix size, OVS, weighted encoding), better separation of lipid peaks (long TE) and possibility to use unsuppressed water (from FID) as an internal reference.

Subjects and Methods
New sequence consists of FID CSI [6] with refocusing pulse after first acquisition (Fig 1). Fat suppression efficiency was tested on cylinder water phantom surrounded by fat layer. Various combinations of matrix size, OVS and encoding were used. Fat contamination was quantified from FID as a ratio of fat signal in magnitude mode to fat and water in every voxel. For in vivo measurement, calf of one volunteer was scanned at 7T Siemens scanner. Parameters of the sequence were TR=1.5s, TE*=1.3ms, TE=280ms, FOV 160x160mm, slice thickness 2cm, 48x48 matrix extrapolated to 64x64 with OVS and elliptical encoding. Spectra in voxels with separated IMCL and EMCL peaks were quantified in AMARES. Concentration with regard to internal water reference from each voxel was calculated after corrections for relaxation for soleus (SM) and gastrocnemius (GM) muscle.

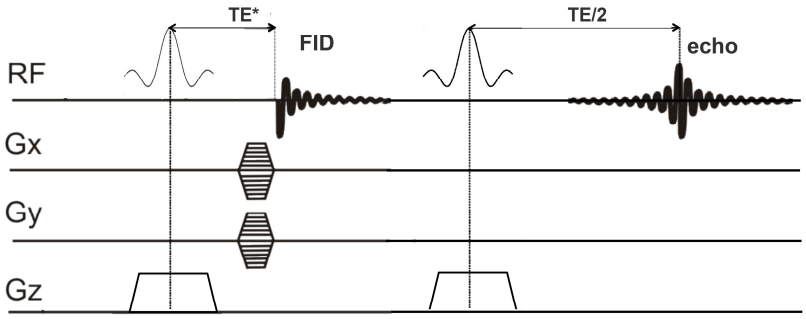

Fig 1. Sequence with FID and echo acquisition in one measurement. Slice selective excitation is followed by two phase encoding gradients, delay of the FID. Refocusing pulse at TE/2 is followed by e water suppression is applied.

Results
Fat suppression efficiency proved to be sufficient (~ 0.66%) with 48x48 matrix extrapolated to 64x64 with OVS and elliptical encoding. In vivo spectra showed fat separation of CH_2 and CH_3 groups for both IMCL and EMCL(Fig 2). Concentration of IMCL in GM were 0.0037±0.0038 and in SM 0.0016±0.0009.

Discussion/Conclusion
As EMCL are known to be present in concentration of two orders of magnitude bigger than IMCL, outer fat contamination needs to be below 1%. *In vivo* spectra with long echo time showed good separation of IMCL and EMCL what allows us to quantify IMCL with the use of water internal reference.

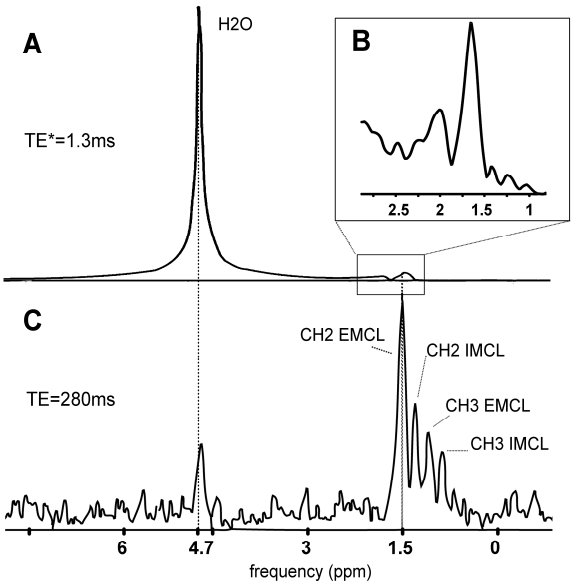

Fig 2. Spectrum acquired at (A) 1.3ms with (B) zoomed area of lipid signal and spectrum acquired at (C) 280ms with water signal almost relaxed but lipid signal separated into four peaks in the range of 0.9-1.5ppm

References
[1] Boesch C et. al. 1997 MRM 484-493
[2] Vermathen P et al. 2004 MRM 253-62
[3] Shen W et al. 2008 NMR Biomed 498-506
[4] Skoch A et al. 2006 JMag Reson Imag 728-735
[5] Ren J et al. MRM 662-671
[6] Bogner W et al. 2010 NMR Biomed 873-882

^{1}H MR Relaxation Times of Lipid Compounds in Liver at 7.0 T

Gajdošík M[1], Chmelík M[1], Bogner W[1], Just Kukurová I[1], Trattnig S[1], Krššák M[2]

1 Centre of Excellence HF MR, Department of Radiology, Medical University of Vienna, Vienna, Austria
2 Division of Endocrinology and Metabolism, Department of Internal Medicine III, Medical University of Vienna, Vienna, Austria

The clinical impact of MRS based liver fat quantification has increased with rising incidence of metabolic disorders especially nonalcoholic fatty liver disease (NAFLD). Liver fat quantification might be of use as a screening tool in patients at risk of NAFLD. Correct spectroscopic quantification requires the knowledge of T_1 and T_2 relaxation behaviour and times. The aim of this study was the assessment T_2 and T_1 relaxation times of hepatic water and lipid compounds at 7T in vivo and evaluating prominent J-coupled resonances with enhanced fitting equation.

Spectra acquired at 7T scanner offered improved SNR. As expected when compared to 3T T_2 relaxation times of liver tissue at 7T are shortened for water and lipids respectively. Water and prominent fat peak (1.3 ppm) T_1 relaxation times at 7T are longer when compared to 3T. The enhanced fitting equation offered higher R^2 with relatively shorter T_2 in most of the cases.

Proton MR Spectroscopic Imaging at 9.4 T: initial results.

Grzegorz L. Chadzynski[1,2], Shajan Gunamony[2], Rupert Kolb[3], Rolf Pohmann[2], Uwe Klose[3], Klaus Scheffler[1,2].

[1]- University Hospital Tübingen, Department of Biomedical Magnetic Resonance, Tübingen, Germany.
[2]- Max Planck Institute for Biological Cybernetics, Department of High-Field Magnetic Resonance, Tübingen,
[3]- University Hospital Tübingen, Department of Diagnostic and Interventional Neuroradiology, Tübingen,

Purpose/Introduction:

Despite of the known difficulties (longer T_1 and shorter T_2 relaxation times, higher SAR and stronger B_0 and B_1 inhomogeneities), the feasibility of in-vivo ^{1}H MRS at a field strength of 9.4 T has been recently demonstrated in [1]. Since the main advantage of CSI over SVS is providing the additional information about the spatial distribution of metabolites, the aim of this study was to examine the feasibility of CSI in the human brain at a field strength of 9.4 T.

Materials and Methods:

In-vivo measurements were performed on a whole body 9.4 T MR scanner (Siemens, Erlangen, Germany). CSI data were collected with a custom built 8 channel transmit coil combined with a 24 channel receiving helmet. Spectra were acquired with a modified STEAM sequence (TR=2000 ms, TE=20 ms, TM=11 ms, spectral bandwidth: 4000 Hz, voxel size: 10 and 5 mm^3 isotropic). The main modification of the pulse sequence consisted in replacing the 90° h-sinc RF pulses with 90° hermite pulses, which allowed keeping the reference voltage below the hardware limitations and minimized the RF power deposition. Raw spectra were quantified with LCModel, version 6.2-2B [2] using a basis set (17 metabolites) simulated in VeSPA software (http://scion.duhs.duke.edu/vespa/).

Results/Conclusions:

Because of the influence of chemical shift displacement, analysis was restricted to the 2 x 2 voxel area in the center of volume of interest. Obtained spectra showed good separation between overlapping metabolite resonances. Quantification with LCModel revealed that it was possible to quantify almost all the metabolites included in the basis set (15 metabolites of the 17 included in the basis set were quantified with CLRB below 20%) All the spectra demonstrated good agreement in terms of spectral resolution and signal-to-noise ratio with the results published previously [1, 3]. In summary we have demonstrated that ^{1}H MRSI at a field strength of 9.4 T is feasible.

References:

1. Deelchand, DK. 2010, J Magn Reson 206, 74-80.
2. Provencher, SW. 1993, Magn Reson Med 30, 672-679.
3. Avdievich, NI. 2009, Magn Reson Med 62, 17-25.

Increasing the SNR in MRSI by Combining the Channels of an Array Coil Using GRE Images for Phasing

Bernhard Strasser, Marek Chmelik, Siegfried Trattnig, Stephan Gruber, Wolfgang Bogner
Medizinische Universität Wien

Using Array Coils (AC) increases the Signal-to- Noise Ratio in comparison to Volume Coils (VC). Yet, the combination of MRSI data of individual channels is problematic due to phase differences between the channels, leading to signal cancellations if the channels are summed naively. The phase information is typically obtained from the first FID point, which can lead to unreliable phase estimation, whereas it is obtained from Gradient Echo (GRE) images in this study.
2D-MRSI data with 64x64x1 voxels of the brains of five volunteers were acquired with an FID-based sequence (acquisition delay of 1.3 ms) at 7T, once with an AC and once with a VC. GRE images with corresponding parameters were measured for phasing and weighting the MRSI data. The SNR between the VC and the AC measurement, using the GRE based coil combination method and the first-FID-point-method, was compared.
The results show an increase in the SNR of 3.2 ± 1.2 when using the AC compared to the VC, and the superiority of the GRE based coil combination over the first-FID-point-method in terms of CRLB values and spectra appearance.

Pulse cascaded Hadamard Spectroscopic Imaging with short acquisition delay in the brain at 7T

G. Hangel, W. Bogner
Medizinische Universität Wien

Recently, pulse-cascaded Hadamard Spectroscopic Imaging (HSI) was proposed for proton-2D-CSI at 7T to reduce maximum B1 amplitude and therefore limit the specific absorption rate. This enables the use of shorter slice selective pulses with higher RF bandwidth, reducing chemical shift displacement errors compared to standard Hadamard encoding. In addition, different groups have shown that proton-2D-CSI can be performed by pulse acquire sequences with short acquisition delay at 7T with excellent quality. This maximizes SNR and avoids J-coupling effects.

Pulse-cascaded HSI-CSI with four slices and standard single slice CSI were compared at 7T to confirm these advantages, the current results show that pulse-cascaded HSI-CSI provides results that are well comparable to standard CSI sequences.

In summary, pulse-cascaded HSI-CSI has a high potential for future multi-slice CSI measurements at 7T.

B_1^+ mapping of ^{31}P coils by steady state CSI

M. Chmelík[1], L. Valkovič[1], M. Považan[1], I. Just Kukurová[1], S. Gruber[1], M. Krššák[2], S. Trattnig[1], W. Bogner[1]

[1] MR Centre of Excellence, Department of Radiology, Medical University of Vienna, Vienna, Austria

[2] Dept. Internal Medicine III, Medical University of Vienna, Vienna, Austria

^{31}P-MRS is primarily applied with sensitive surface coils that provide inhomogeneous B_1^+ excitation and rough localization due to their B_1^+/B_1^- profile. careful and time-consuming pulse adjustments, as well as an accurate knowledge of flip angle (FA) distribution (acquired empirically or calculated via computer simulation) and T_1 relaxation times, is mandatory for quantification corrections.

We adapted pulsed steady state method (also known as double TR method) described by Yarnykh (MRM, 2007) for use with phosphorus setup. Flip angle (FA) maps were acquired in localization phantom using surface coil and breast coil for two pulse types – conventional Sinc3 pulse with durations 600us and 1280us and adiabatic AHP pulse with duration 2500us. 2D and 3D CSI (16x16 and 16x16x16 voxels) sequences with two different repetition times were measured for each pulse type, in case of conventional pulse TR1=0.5s and TR2=3s, in case of AHP pulse TR1=1.4s and TR2=4s. The observed signals S1 and S2 are proportional to the longitudinal magnetization) and their ratio is given by:

$$\frac{S_1}{S_2} = \frac{\frac{M_0(1-e^{-TR1/T_1})}{(1-cos(\alpha)e^{-TR1/T_1})}}{\left(\frac{M_0(1-e^{-TR2/T_1})}{(1-cos(\alpha)e^{-TR2/T_1})}\right)} \quad \text{then} \quad \alpha = arccos\left(\frac{1-e_1-r+re_2}{e_2-re_1+re_1e_2-e_1e_2}\right)$$

where $r = \frac{S_1}{S_2}$ and $e_1 = e^{-TR1/T_1}$, $e_1 = e^{-TR2/T_1}$

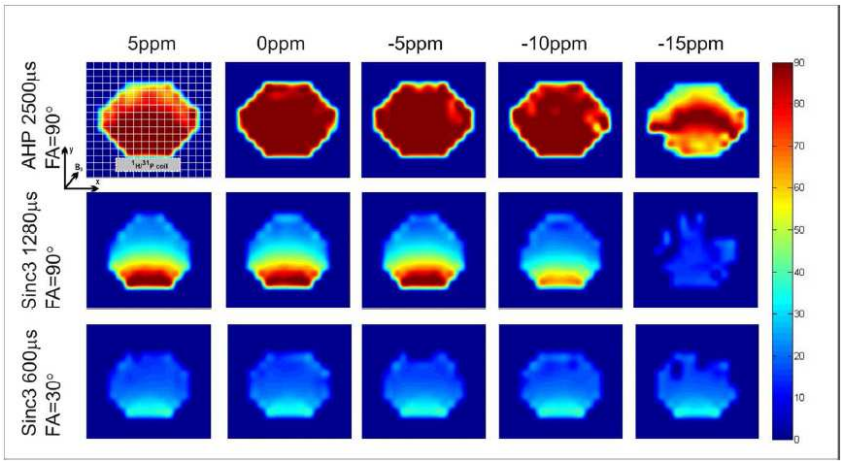

Fig.1. Experimentally determined FA maps of a 2.5-ms long 90˚ AHP (top row), a 1.28-ms long 90˚ Sinc3 (middle row), and a 0.6-ms
long 30˚ Sinc3 pulse used for excitation for 5, 0, 5,-10, and -15 ppm offsets.

Introduced method enables direct measurement of FA maps in phantoms and may be easily used even during in vivo ^{31}P protocols.

Monday, June 25, 2012

16:00-18:00 Scientific session 2

From straight to inverse fMRI retinotopic mapping
C. Segebarth

UMPIRE: a new method for unwrapping multi-echo phase images
S. Robinson, H. Schödl and S. Trattnig

UMPIRE: implementation and results
H. Schödl S. Trattnig, S. Robinson

Stimulation with Chirp-pulses in fMRI measurements of the auditory pathway
M. Ryn, M. Erb, U . Klose

Topology and frequency characteristics of the auditory cortex during aging: A fMRI study
J. Tintera, I. Ibrahim, Z. Balogova, O. Profant, J. Syka

FMRI of the visual system – from straight to inverse retinotopic mapping.

Christoph Segebarth – INSERM U836, Grenoble, France

I will present the principles of an fMRI application I have been involved with for some years - fMRI retinotopic mapping. FMRI retinotopic mapping usually relies upon Fourier analysis of functional responses to periodic visual stimuli that encode eccentricity or polar angle in the visual field. Generally, phase estimates of the responses are assigned to a surface model of the cerebral cortex and borders between retinotopic areas are eventually determined following *ad hoc* phase analysis on the surface model – at the border between adjacent visual areas, the cortical representation of the polar angle in the visual field is inverted (so-called inversion of the "visual field sign") and this inversion is reflected in the phase properties of the fMRI signals.

We have recently applied retinotopic mapping with the view of enhancing significantly the (group) detection sensitivity of the functional responses in low level visual areas obtained in cognitive experiments on the visual system. We therefore project the individual functional responses (of the cognitive experiment) detected in low level visual areas onto frames corresponding to the visual field (we thus perform so-called "inverse retinotopic mapping"). For each individual, we thus obtain one functional map per retinotopic area that has been delineated in a preliminary fMRI delineation experiment. Importantly, each of these maps is represented in the coordinate system of the visual field. In doing so, we get rid of the sensitivity to inter-individual anatomic and anatomo-functional variability. We hypothesize that this approach will enhance significantly the detection sensitivity in group analyses, as compared to the conventional approach whereby individual responses are warped onto a common anatomical template.

Reference: J.Warnking et al. FMRI retinotopic mapping – step by step. NeuroImage 2002; 17(4): 1665-83.

UMPIRE: a new method for unwrapping multi-echo phase images

Simon Robinson, Horst Schödl and Siegfried Trattnig

Medizinische Universität Wien

Purpose/Introduction

MR phase values outside a 2π range are aliased, causing phase images to contain discontinuities, or "wraps". Wraps can be removed with spatial, region-growing methods [e.g. 1] which, however well implemented, are computationally intensive and inherently not very robust. Alternatively, the evolution of phase over time can be used to identify wraps on a voxel-by-voxel basis - a temporal approach. Temporal unwrapping requires two or more phase values but is more reliable. Generally the echoes need to be acquired in separate single-echo acquisitions so that echo time differences can kept small enough that the phase difference between echoes is less than 2π. The aim of this study was to develop a temporal unwrapping method that works with multi-echo scans at ultra-high field, where a number of wraps may occur between echoes. The resulting approach is called UMPIRE, or Unwrapping Multi-echo Phase Images with iRregular Echo spacings.

Subjects and Methods

Multi-echo gradient-echo scans (2x2x2mm) were acquired with a 7T Siemens system with TEs={5.0,10.0,16.0}ms, i.e., with an additional delay (δTE) of 1ms between the second and third echo. UMPIRE was implemented in MATLAB. Phase images (P) were reconstructed (Fig.1-A) using the MCPC-3D-II method [2]. Phase difference (PD) images were calculated between pairs of phase images (Fig.1-B). The difference between these phase difference images (DPD) was also calculated (Fig.1-C). DPD is free of wraps if δTE is sufficiently short. Wraps in PD images were identified by comparison with DPD (Fig.1-D), and removed (Fig.1-E). Unwrapped PD images were used to re-estimate (with improved SNR) the rate of phase change (Fig.1-F) – analogous to step C. The re-estimate of rate of phase change was used to identify (Fig.1-G) and remove wraps in these (Fig.1-H) to complete the process.

Results

UMPIRE removed phase wraps in all voxels in which the phase change in time δTE (which can be chosen at will) was below 2π. UMPIRE required 2.2s for calculation, compared to the spatial method PRELUDE [1] which took 321s in 3D mode and 8.3s in 2D mode (which leaves phase jumps between slices).

Discussion/Conclusion

The use of unequal spacings between echoes in UMPIRE allows phase images to be unwrapped despite a number of wraps being present between echoes. Further speed advantage over spatial methods is expected with implementation in C. UMPIRE is fast and allows phase wraps to be reliably removed in multi-echo acquisitions such as field mapping [3] and multi-echo SWI [4].

References

1. Jenkinson M. Fast, automated, N-dimensional phase-unwrapping algorithm. Magn Reson Med 2003;49(1):193-197.
2. Robinson S, Grabner G, Witoszynskyj S, Trattnig S. Combining phase images from multi channel RF coils using 3D phase offset maps derived from a dual-echo scan. Magnetic Resonance in Medicine 2011;65:1638-1648.
3. Robinson S, Jovicich J. B0 mapping with multi-channel RF coils at high field. Magn. Reson Med 2011;66(4):976-988.
4. Denk C, Rauscher A. Susceptibility weighted imaging with multiple echoes. J Magn Reson Imaging 2009;31:185-191.

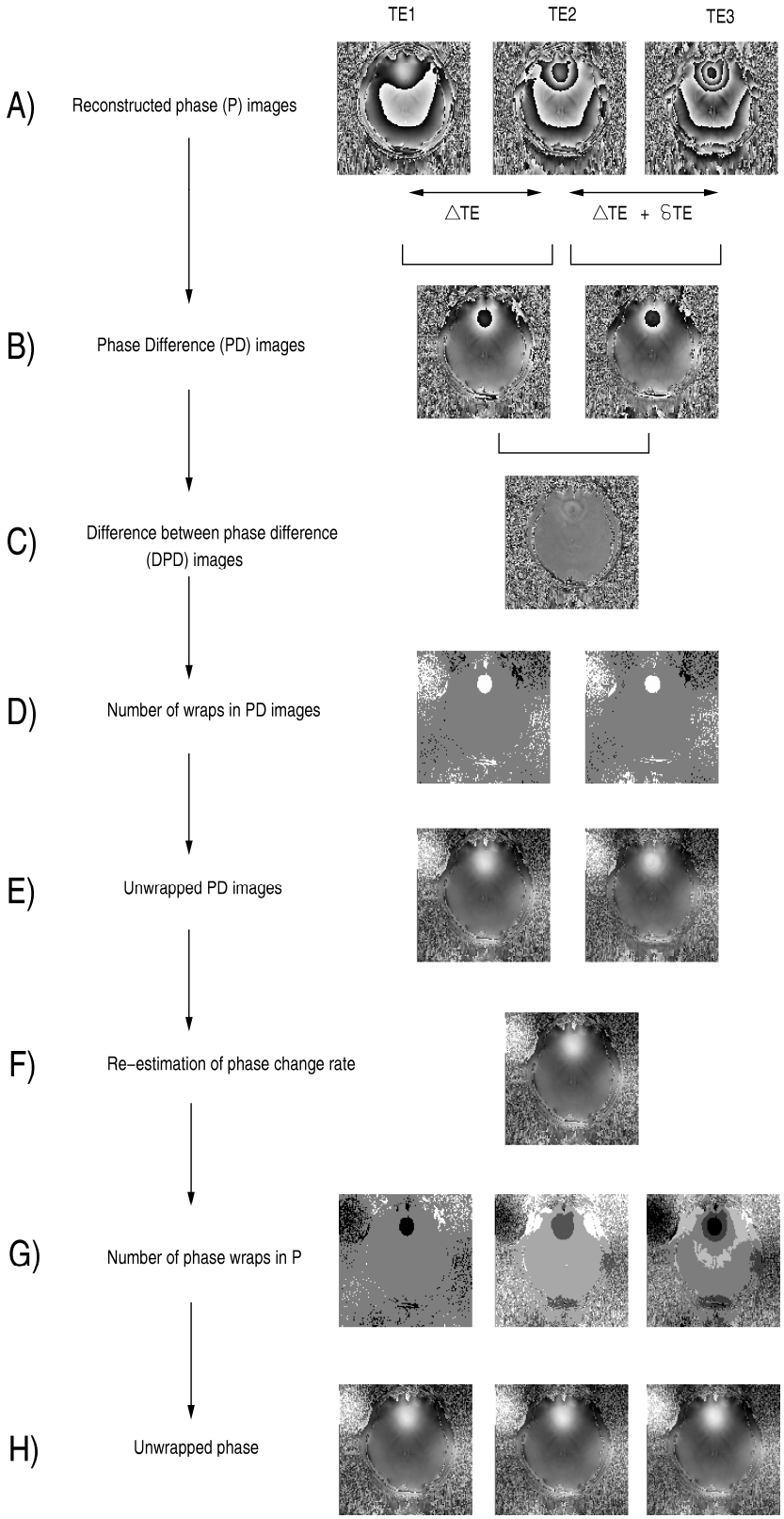

Figure 1: Steps in the UMPIRE method, described in the text.

UMPIRE: Implementation and results

Horst Schödl, Simon Robinson, Siegfried Trattnig

High Field MR Center of Excellence, Department of Radiology, Medical University of Vienna, Austria.

Introduction
UMPIRE is a temporal phase unwrapping method which identifies wraps on a voxel-by-voxel basis. The approach aims to unwrap a number of wraps between echoes in multi-echo acquisitions, as typically occur at ultra-high field in such applications as field mapping and multi-echo SWI. The steps in UMPIRE are explained in another talk at this workshop [1]. This presentation focuses on the implementation of UMPIRE in C and a comparison of UMPIRE with spatial unwrapping methods.

Measurements
Three triple echo gradient-echo scans (2x2x2mm) were acquired with a 7 T Siemens system with TE1=5.0 ms, TE2=10.0 ms and TE3=15.3, 16.1 and 16.9 ms, i.e., with additional delays between the second and the third echo (δTE) of 0.3, 1.1 and 1.9 ms respectively. Image quality was performed by eye, assessing discrepancies between UMPIRE and spatial unwrapping results (noise and voxels which were not correctly unwrapped) in order to establish the optimum δTE.
In PHUN [2] and PRELUDE [3] a threshold - a specified signal level in the corresponding magnitude image - is set which determines which areas of the object to unwrap. Since UMPIRE identifies wraps voxel-by-voxel no threshold is needed. The calculation time for different threshold levels was compared between UMPIRE and spatial unwrapping methods PHUN (2D) and PRELUDE (both in 2D and 3D mode).

Results
At very short δTE (0.3 ms), the phase difference between echo pairs is small, so no wraps occur, but the SNR in the estimation of phase precession rate (DPD – see [1]) is low and unwrapping in regions of signal dropout may not succeed. For higher δTE (1.9 ms) the SNR is higher but wraps remain in regions when the phase evolution in time δTE exceeds 2π. The optimum value for δTE is found to be around 1 ms for 7 T and the brian regions considered. UMPIRE required 1.097 ± 0.003 seconds to unwrap all three phase images, PHUN required 2.150 ± 0.175 seconds and PRELUDE 2D and 3D used 9.825 ± 0.017 seconds and 20m 29.315 ± 34.351, respectively.

Discussion
UMPIRE has some clear advantages compared to the other methods: all 2D-unwrapping methods leave phase jumps between slices, which don't occur with UMPIRE. The 3D calculation with PRELUDE takes significantly longer and fails on unconnected regions of the image.

Conclusion
UMPIRE is a fast method for unwrapping multi-echo images. UMPIRE does not need a seed region or for there to be connection between regions to be unwrapped, meaning that it works with a number of separate objects. It unwraps all voxels, not just those identified to be within the object (those with high SNR). The measurements show a significant advantage in calculation time over spatial methods. UMPIRE is based on phase differences, so it may

perform worse than spatial methods in regions of low SNR. Further improvements in speed and robustness in removing wraps appearing due to fast phase changes are planned.

References

[1] Simon Robinson, Horst Schödl and Siegfried Trattnig, 2012, UMPIRE: a new method for unwrapping multi-echo phase images. Abstract for the workshop Prag-Tübingen-Vienna in Oberschwarzenberg.
[2] S. Witoszynskyj, A. Rauscher, J. R. Reichenbach, M. Barth, 2009, Phase unwrapping of MR images using Phi UN--a fast and robust region growing algorithm. Medical Image Analysis; 13:257-268.
[3] Jenkinson M. 2003, Fast, automated, N-dimensional phase-unwrapping algorithm. Magnetic Resonance in Medicine 2003;49(1):193-197.

Stimulation with Chirp-pulses in fMRI Measurements of the Auditory Pathway

Michalina Ryn [(1)], Michael Erb [(2)], Uwe Klose [(1)]

Department of Diagnostic and Interventional Neuroradiology, University Hospital of Tübingen [(1),] Department of Biomedical Magnetic Resonance Imaging, University Hospital of Tübingen [(2)],

The chirp is a special auditory acoustics stimulus in which the high-frequency components are delayed relative to the low-frequency components in appropriate amount. These broad band stimuli with tonotopic temporal delay, not only, increase neural synchrony at peripheral and central levels, but also increase the neural activity in the brainstem. A chirp stimulus is now used in Auditory Brainstem Reponses (ABR). The results shows that the signal amplitude of chirp-ABRs is two times larger compared to click-ABRs. This means that there are more neurons activated at same time. Up till now there are no fMRI studies which used this kind of stimulus for visualization of auditory pathway. The purpose of this study was to investigate the effect of binaural chirp stimuli on auditory brainstem using fMRI technique with normal hearing subjects. Presented study showed very high detection rate for visualization structures in brainstem (almost 100%) compared with previous studies (80 %). It is the first time that a chirp stimulus was used in auditory fMRI to detect subcortical activations. The location of cortical and subcortical regions of auditory pathway corresponds well with the location of the particular activations in data of other fMRI studies within auditory pathway.

Topology and frequency characteristics of the auditory cortex during aging: A fMRI study

J. Tintera, I. Ibrahim, Z. Balogova, O. Profant, J. Syka

IKEM, Prague

Purpose
The study evaluated age related differences in brain activation of the auditory cortex using fMRI and auditory stimulation with various frequencies.

Methods
All healthy subjects with signed informed consent were divided into three groups: A-young (average age 24y), B-old normal (average age 69y) and C-old with increased presbyacusis (average age 72y). The threshold to distinguish subjects with normal and increased presbycusis was set at 25% of distribution function according to ISO 7029 standard. Each group consisted from 18 subjects.
All fMRI examinations were performed on Siemens Trio 3T scanner using 12-channel head coil and GRE-EPI sequence: TE=30ms, TR=8s, α=90°, voxel 3x3x3mm, 30 slices.
An event-related design and sparsely data acquisition were used. Each event of auditory stimulation lasted 6 sec and was conducted via MR compatible audio system MR-Confon HP SC01. Stimulation itself realized third-octave pink noise with five centre frequencies: 350 Hz, 700 Hz, 1.5 kHz, 3 kHz, 8 kHz. All frequencies were applied during single measurement in pseudo-random order (10 stimulations for each frequency). Measurements contained 152 dynamics and lasted 20 min.
Evaluation was done in SPM8 (realignment, slice timing, smoothing to 6x6x6mm and GLM). Group statistic was calculated (t-test, p=0.05 FWE correction) was used for each group and all frequencies. Difference between groups was tested with two-sample t-test and uncorrected threshold of p=0.001.

Results
Activations in auditory cortex were slightly shifted from in medial direction with increasing frequency but these areas were extensively overlapped (fig. 1). Number of activated voxels decreased in higher frequency for all groups but strongly in both older groups, significant drop of activation was seen at 8 kHz in group C. In lower frequency, the activation was larger in older subjects (both groups) but in the highest frequency more activation in young subjects was found (fig. 2). This situation was also confirmed with statistical analysis by testing the difference of the activation between groups. Only positive voxels of higher activation in older subjects over young group were found in auditory cortex (B>A and C>A) while we found no difference between old groups and also no significantly greater activation in young subjects (A>B, A>C) – fig.3.

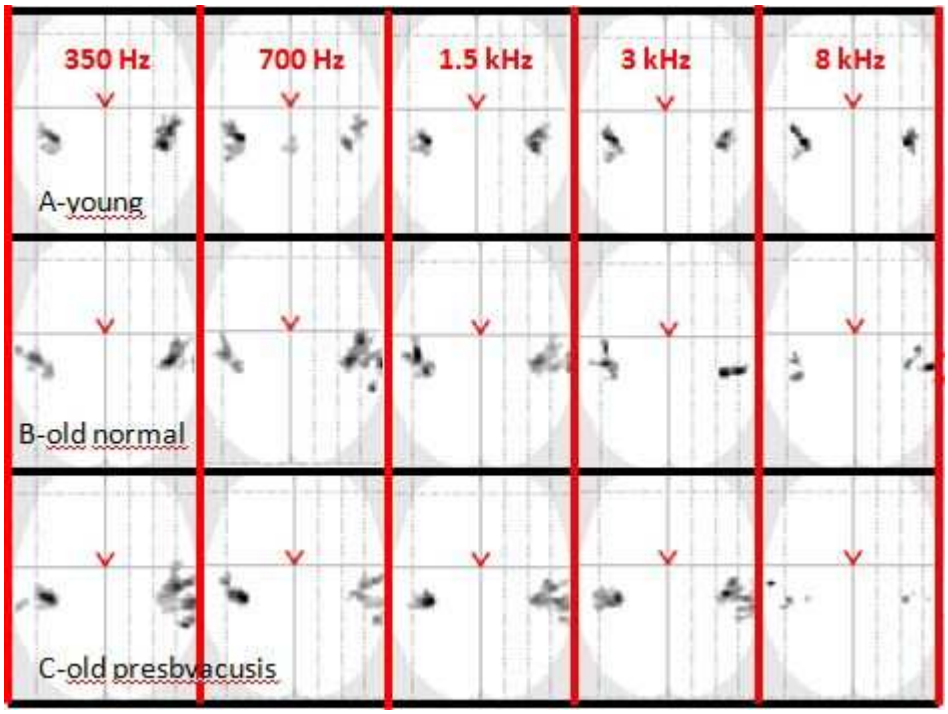

Fig.1 Activations on five frequencies (columns) and three groups (lines)

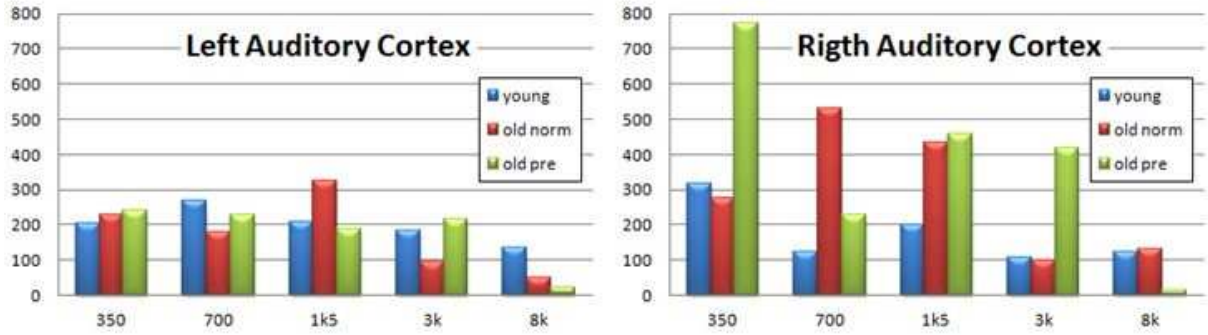

Fig.2 Number of active voxels at all frequencies

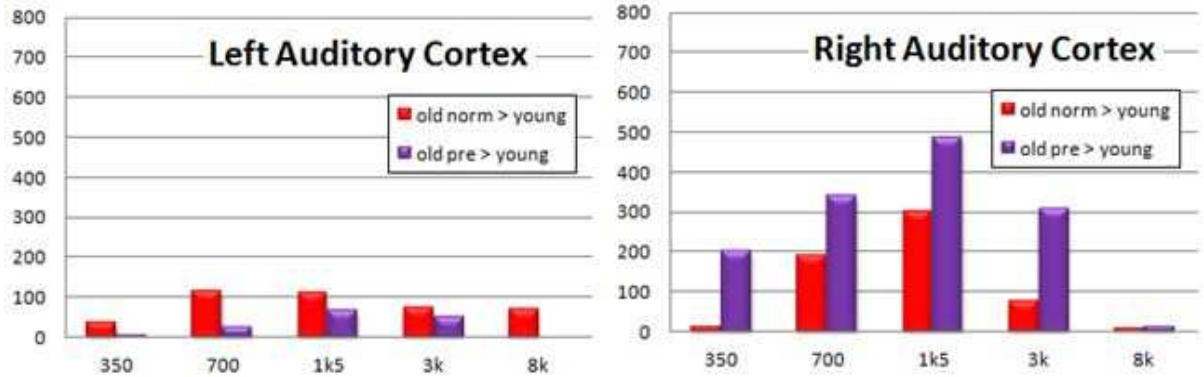

Fig. 3 Statistical difference in activation [voxels] (p=0.001 uncrorr.)

Conclusion: With the exception of the highest tested frequency, the amount of activated voxels was higher in older subjects, more prominently in the right hemisphere.

Acknowledgements

Supported by GACR P304/10/1872 and MZCR Institutional project 00023001 IKEM.

Monday, June 25, 2012

20:00-21:30 Scientific session 3

High Field MR Spectroscopy on Rodents
V. Mlynárik

Small monkeys and big machines: Multimodal SPECT and MRI of the Common Marmoset using clinical hardware.
G. Helms

Personalized medicine: the view of patients, physicians and politicians
M. Hájek

High-field MRS of rodents

Vladimír Mlynárik

Laboratory of Functional and Metabolic Imaging, Ecole Polytechnique Fédérale de Lausanne, Lausanne, Switzerland
Email: vladimir.mlynarik@epfl.ch

Rats and mice serve as subjects for modeling various pathological conditions, which can be studied by localized MR spectroscopy. Measurements at high magnetic fields benefit from the higher signal-to-noise ratio and increased spectral dispersion, which improves quantification accuracy and precision. The benefits are expected to be important especially for metabolites having low concentration or overlapping spectral lines and for compounds giving complex J-coupled spectral patterns.
For obtaining reliable information on metabolite concentrations in rodent brain, well-resolved short-echo-time spectra are necessary, which are not contaminated by MR signals coming from outside the volume of interest and have undistorted baseline, e.g., due to large residual water peak. To achieve these goals, a stable magnet with eddy current compensated gradients, a powerful shimming method and an optimized pulse sequences should be used. In addition, a robust spectra quantification software is necessary for obtaining accurate metabolite quantification.

The increased sensitivity at a high magnetic field is also beneficial for proton spectroscopic imaging. This technique reduces chemical shift artefacts and can shorten the total measurement time, when spectra from different brain regions are to be measured.

Small monkeys in big machines

Gunther Helms

Göttingen, Germany

The common marmoset monkey (Callithrix jacchus) is increasingly used as a model for neurodegenerative diseases. We established a comprehensive protocol of 3D structural and FLASH-based quantitative MRI for the marmoset brain on a 3T clinical MRI system using the wrist coil.
An isotropic resolution of 0.4 mm yielded sufficient SNR within the 30 minutes time frame of injection anesthesia, whereas 0.33 mm require inhalation anaesthesia. Applications pertain to anatomical correlates of DAT-SPECT, the excretion of gadolinium contrast agent and the EAE model for multiple sclerosis.

Personalized medicine: the view of patients, physicians and politicians

Milan Hájek

IKEM, Prague

Definition: "Personalized medicine is the tailoring of medical treatment to the individual characteristics of each patient. The approach relies on scientific breakthroughs in our understanding of how a person's unique molecular and genetic profile makes them susceptible to certain diseases. This same research is increasing our ability to predict which medical treatments will be safe and effective for each patient, and which ones will not be."
We will discuss different opinions to personalized medicine and look for the application of MR methods in this field.

Tuesday, June 26, 2012

8:30-10:10 Scientific session 4

Tracking the Fate of SPIO-Labeled transplanted rat pancreatic islets: the animal model matters
D. Jirák, K. Zacharovová, Z. Berková, V. Herynek, E. Dovolilová, F. Saudek, M. Hájek

Ex vivo MR microimaging and histology of neuronal damage in rat model of vascular dementia
A. Gálisová, M. Krššák, C. Kronnenwetter, A. Berg, I. Sadloňová , A. Kebis, K. Ambrušová, S. Kašparová

The quantification of ^{1}H MR spectra from rat brain with modeled vascular dementia including simvastatin therapy by QUEST
M. Jozefovičová, K. Černý, T. Liptaj, S. Kašparová

Dendrochronology based on high-resolution Magnetic resonance imaging
A. Berg, R. Fürhacker, A.-K. Klatz, M. Grabner

Sodium imaging at 9.4 T
C. Mirkes

Tracking the Fate of SPIO-Labeled transplanted rat pancreatic islets: the animal model matters

Daniel Jirák[1], Klára Zacharovová[2], Zuzana Berková[2], Vít Herynek[1], Eva Dovolilová[2], František Saudek[2] , Milan Hájek[1]

[1]Laboratory of Langerhans Islets, Centre of Experimental Medicine, Institute for Clinical and Experimental Medicine, Prague, Czech Republic
[2]MR Unit, Department of Diagnostic and Interventional Radiology,
Institute for Clinical and Experimental Medicine, Prague, Czech Republic
[3]Biology Centre ASCR, Institute of Parasitology, Czech Republic

Introduction: Superparamagnetic iron oxides (SPIO) labeling of isolated pancreatic islets enables their long-term post-transplant monitoring by magnetic resonance imaging (MRI). Although the nanoparticles are incorporated into all major islet cell types during in vitro culture, little is known about their fate in vivo. We studied the morphology of labeled islets after transplantation to identify the relation between observed MRI contrast and transplantation outcome.

Methods: Rat Lewis islets labeled with the SPIO contrast agent ferucarbotran were transplanted via portal vein into the liver, or under the kidney capsule of syngeneic and allogeneic rats (Brown Norway rats). MRI of anesthetized animals was performed using a 4.7T MR scanner 1, 2, 4 weeks after transplantation. Morphology of the transplanted tissue was studied by light, fluorescence and transmission electron microscopy at different time points for up to three months.

Results: Morphology of syngeneic islets transplanted beneath the kidney capsule and into the liver was similar. Iron particles were almost completely eliminated from the endocrine cells and located in host-derived macrophages surrounding the vital islets; the particles persisted at the transplantation site for the entire study period. In the allogeneic model, islets lost their function and were rejected within nine days following transplantation in both transplant sites. However, intercellular transport of the SPIO particles and subsequent MRI findings were different in the liver and kidney. In the liver the decreasing number of islet-related MRI spots corresponded with clearance of iron particles in rejected islets; in contrast, in the case of renal transplants, extensive iron deposits with a high effect on MRI signal persisted in phagocytic cells beneath the renal capsule for up to two months.

Conclusions: Although the SPIO particles were located aside the endocrine cells after islet transplantation, MRI detection of the contrast agent correlated with islet survival and function in islet transplantation into the liver. However, it did not correlate in the case of transplantation beneath the renal capsule. Therefore, MRI can be reliably used for immediate confirmation of the transplantation success tissue both in the liver and kidney, but monitoring over time is effective only within the liver.
Supported by grants MZO 00023001 and ENCITE 7th Framework Program EU (No.: 201842) .

Ex vivo MR microimaging and histology of neuronal damage in rat model of vascular dementia

Andrea Gálisová[1], Martin Krššák[2], Claudia Kronnenwetter[2], Andreas Berg[2], Irina Sadloňová [3], Anton Kebis[4], Katarína Ambrušová[4], Svatava Kašparová[1]

[1] Faculty of Chemical and Food Technology, Slovak University of Technology, Bratislava, Slovakia
[2] MR Centre of Excellence, Department of Radiology, Medical University of Vienna, Vienna, Austria
[3] Department of Toxicology, Hameln r.d.s., Modra, Slovakia
[4] Slovak Medical University, Bratislava, Slovakia

Chronic cerebrovascular insufficiency associated with advanced aging may play a causative role in the pathology of sporadic Alzheimer's disease (AD) [1]. We use a pathophysiological model of vascular dementia (VD) which was confirmed as a suitable model mimicking AD-like pathology [2]. The aim of this study was to assess the hallmarks of AD, like the amyloid plaques and neuronal loss, by means of *ex vivo* MR microimaging (MRMI) without the use of contrast agent and comparison with histology. MR imaging was conducted on the 7T Siemens scanner with the 750mT/m gradient coil insert and the 19mm volume resonator. 3D T_2-weighted images were obtained by turbo spin echo sequence with spatial resolution of $44x44x200\mu m^3$ (TR=3000ms, TE=83ms, ETL=19). Although no individual plaques were detected, images revealed differences between control and VD group in MR contrast of

cortex, ventricles and CA1, CA3 pyramidal cells and granular cells in hippocampus and an elevation of T_2 times was found in these areas. After MRMI measurements, the rat brain samples were histologically stained with hematoxylin and eosin. Changes observed in MR images were in agreement with histological findings of necrotic neurons in the CA1 layer. Our results demonstrate the ability of MRMI to distinguish between healthy and damaged tissue of rat brain on microscopic level and provide a detailed view of rat brain anatomy highlighting also different hippocampal subfields.

Acknowledgement: Financial support from the Grant Agency VEGA of the Slovak Ministry of Education, grant No. 1/0272/10, and from the bilateral programme Action Austria – Slovakia, Co-operation in Science and Education, grant No. 2010-10-15-9014.

References:

[1] de la Torre, J.C., 2004, Lancet Neurol, 3:184
[2] Horecký, J. et al., 2009, J Neurol Sci, 83:178-183

The quantification of ^{1}H MR spectra from rat brain with modeled vascular dementia including simvastatin therapy by QUEST

Jozefovičová M.[1], Černý K.[2], Liptaj T.[1], Kašparová S.[1]

[1] Faculty of Chemical & Food Technology, Slovak University of Technology Bratislava, Slovakia
[2] MR- unit, Department of Radiodiagnostic and Interventional Radiology, Institute for Clinical and Experimental Medicine, Prague, Czech Republic

The quantification of *in vivo* proton MR spectra measured from the rat brains provides important information about the metabolite concentrations and can help to understand the role of the metabolites under normal and pathological conditions or treatment effect.
Many algorithms for quantification of the signals presented in proton *in vivo* MR spectra have been proposed. We use the QUEST algorithm (QUantitation based on QUantum ESTimation –jMRUI) based on time domain. Proton MR spectra were measured in aged rat brains (15-months old Wistar rats) from three groups (control, with vascular dementia [1] and group with vascular dementia treated with simvastatin). Single voxel localized spectroscopy with short echo time (SPECIAL, TE = 2.8ms, voxel size: 3x4x5mm) was used for spectra acquisition [2]. The aim of this study was to use the algorithm QUEST for quantification of these three groups of ^{1}H MR spectra and their comparison. The results and the problems associated with quantification are discussed.

Acknowledgement:
Financial support from the Grant Agency VEGA of the Slovak Ministry of Education, grant No. 1/0272/10.

References:

[1] Ferreira E.D.F. et al., EJN 1, 10 (2011)
[2] Mlynárik V. et al., MRM 56:965 (2006)

Dendrochronology based on high resolution Magnetic Resonance Imaging ?

A. Berg[1], R. Fürhacker[2], A.-K. Klatz[2], M. Grabner[3]

[1]Vienna/AT, [2]Gutenberg An der Raabklamm/AT, [3]Tulln/AT

Archaeological finds represent very valuable pieces of documentary evidence for human history and cultural development and do in many cases deserve conservation without using destructive dating - or analyzing methodology. MR-imaging is competing with x-ray and ultrasound with regard to the non-invasive visualization of the inner structure and morphology not only in medical applications but also in material science. Is it possible to use MR-imaging modality not only with regard to ancient human samples ("Oetzi") but also for the non-invasive detection of the annual ring (AR) periodicity in archaeological wood? An accurate detection of this periodicity would in principle allow for the archaeological dating of the corresponding wood sample using statistical correlation to known and already available dated AR-patterns (Dendrochronology). The MR-based AR-data may also be relevant for dendro-climatology, dendro-ecology and micro-characterization of the wood species, relevant for conservation.

We present here, to our knowledge for the first time, high-resolution MRI-data on wet wood specimen relevant for dendrochronology. The samples of different size (≅1-100cm) originate from a middle bronze age (≅1500 b.C.) well recently discovered in Wohlsdorf /Steiermark /Austria.

The variety of different wood species and sediments in these samples demands for an extensive diversity of hardware, pulse-sequences and MR-protocols ranging from Ultra-High-Field (UHF) large scale imaging (cp-head-coil, i.d.28 cm), down to microscopic spatial resolution, from T2-mapping at standard echo-times of ms down to Ultra-short-Encoding-Time (UTE) imaging (TE=70μs).

A short overview of the different MRI-methodologies and results is presented giving evidence for the possibility of MRI-based dendrochronology as proof of principle.

Sodium imaging at 9.4 T

Christian Mirkes

Dept. for Biomedical Magnetic Resonance, University of Tübingen, Tübingen, Germany
Max Planck Institute for Biological Cybernetics, Tübingen, Germany

Although hydrogen is the most commonly imaged nucleus in magnetic resonance imaging (MRI) due to its high concentration in biological tissues in the form of water and fat, any other nucleus having a net nuclear spin, such as sodium (^{23}Na), can be used for imaging and potentially gaining additional information. Even though sodium is the second most abundant MR active nucleus in the human body, the signal produced by it is considerably lower than the one obtained from hydrogen. This is due, on the one hand, to the underlying physics characterising the relaxation of the excited sodium nucleus and, on the other hand, to the 1000 fold lower *in vivo* concentration. The inherently low signal-to-noise ratio can be considerably enhanced by using dedicated non-Cartesian ultra-short echo time sequences and MR scanners with ultra-high magnetic field strengths. The concomitant increase in sensitivity permits the acquisition of sodium images exhibiting a higher spatial resolution than would be possible with standard sequences and low field MR scanners, while maintaining a clinically acceptable scan time. As sodium ions play an important role in cellular homeostasis and cell viability, ^{23}Na MRI can serve as a means for the assessment of cell integrity. Furthermore, sodium imaging might prove to be a powerful diagnostic tool in the future to quantify degenerative changes, e.g. in articular cartilage.

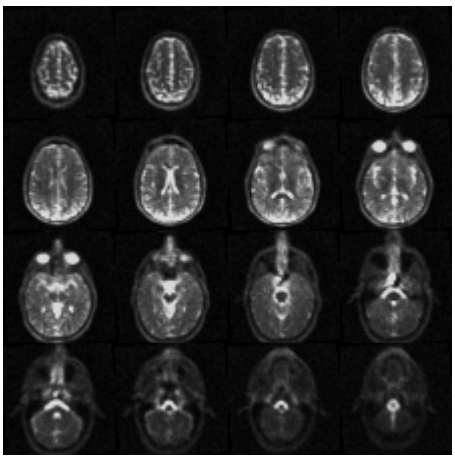

Figure 1: Sodium images of a healthy human brain acquired with a Siemens (Erlangen, Germany) 9.4 T whole-body scanner using twisted projection imaging at a nominal isotropic resolution of 2 mm.

Tuesday, June 26, 2012

10:30-12:30 Scientific session 5

fMRI with spin-echo EPI sequences
A. Zawadzka, M. Ryn, U. Klose

Distortion-free high-resolution fMRI at 9.4 T
P. Ehses, J. Budde, G. Shajan, K. Scheffler

uN-BIASED: a nearly model-free fMRI analysis method based on reproducible responses and applied to 7 T clinical fMRI
P. Cardoso, A. Geissler, F. Fischmeister, S. Trattnig, R. Beisteiner, S. Robinson

Stability of intraindividual resting-state measurements
M. Erb

Resting state evaluations in a group of MS patients
E. Charyasz, B. Bender, U. Klose

Analysis of resting state signal variations in patients with Friedreich ataxia
M. Löffler

---

fMRI of the auditory cortices with spin-echo sequences

A. Zawadzka, M. Ryn, U. Klose

This study is performed in order to compare the activation in auditory pathway, measured with the conventional gradient-echo EPI sequence and with spin-echo EPI sequence. SE-EPI, due to the presence of refocusing pulse, has the ability to restore the signal mainly in capillaries. Therefore, a higher spatial localization of foci of activation is expected.

Data of three subjects were analyzed in a five different sessions. First experiment was a standard GE-EPI experiment. Further SE-EPI measurements were performed with two different echo times and gated and not-gated. The repetition time depended on a cardiac cycle or set as a stable.

Bilateral activation in auditory cortex was obtained within the use of both techniques. The highest t-value, cluster size and a time-course analyses have been analysed. Although the activation for SE-EPI was considerably weaker than for GE-EPI, it had enabled a visual distinction of different cortical areas, contrary to GE results.

Distortion-free high-resolution fMRI at 9.4 T

Philipp Ehses[1,2], Juliane Budde[2], G. Shajan[2], Klaus Scheffler[1,2]

[1]Department for Neuroimaging, University Hospital Tübingen, Tübingen, Germany
[2]Max Planck Institute for Biological Cybernetics, Tübingen, Germany

Introduction: SNR benefits allow for significantly higher resolution in BOLD fMRI at ultra-high fields. On the flip side, faster T_2^* relaxation leads to blurring and increased B_0 field inhomogeneities aggravate distortion artifacts in EPI BOLD imaging at higher fields. Both of these problems can be alleviated by shortening the EPI read-out using parallel imaging and/or segmentation. In the extreme case, only a single echo is acquired in every TR, transforming the EPI into a conventional gradient-echo (GRE) sequence. The aim of this work is to develop an effective single-echo GRE sequence for BOLD fMRI at ultra-high magnetic field. To this end, echo-shifting (ES) [1] was combined with an interleaved slice order, in order to optimize echo time, scan time, and SNR for multi-slice BOLD fMRI.

Methods: All experiments were performed at 9.4 T on a healthy volunteer with informed consent and IRB approval. A custom-built head coil was used for signal transmission/reception (8 transmit / 18 receive channels). An echo-shifted GRE with interleaved slices was developed, similar to a recently proposed EPI-based sequence [2]. Parallel imaging (R=2) and partial Fourier (6/8) were used to accelerate image acquisition. Other sequence parameters were as follows: FA = 22°, effective TR/TE = 80/20 ms with ten interleaved slices and two echo-shifts, slice thickness = 1 mm, 1 mm in-plane resolution, TA per repetition = 4.32s, 70 repetitions, total TA = 5min. The paradigm consisted of finger tapping with the right hand, alternating between 20s of rest and 20s of tapping. For analysis, the data were processed with FSL FEAT. Data processing was repeated with and without spatial smoothing, using a Gaussian filter kernel (FWHM=1mm). In addition, a high-resolution GRE image served as a reference (FA=25°, TR/TE=500/14ms, resolution=0.23x0.23mm², slice thickness=1mm, 16 slices). Activation maps were registered to this reference using a six-parameter rigid body model.

Results: Figure 1ab shows an overlay of the smoothed activation map over a) the averaged raw image and b) registered to the reference image. In Figure 1c-e, an overlay of the left motor cortex with activation maps with and without smoothing is shown. The position of veins close to the motor cortex strongly correlates with high BOLD activation.

Discussion/Conclusion: The results show that the proposed method is well suited for high-resolution fMRI at ultra-high magnetic field. Advantages compared to EPI are that it results in less T_2^* blurred and virtually distortion-free images. This comes at the cost of longer scan times (4.32 s for 10 slices vs. 2s for a typical >=20 slices EPI). Further optimizations and higher acceleration factors may help to close this gap, although we believe that EPI will remain more time-efficient.

References: [1] Moonen et al. MRM 1992;26:184-9. [2] Gibson et al. Magn Reson Imaging 2006;24:433-42.

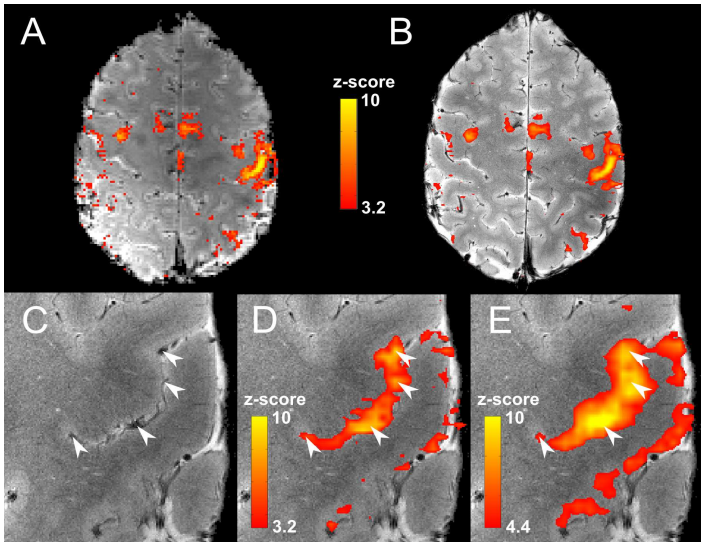

Fig 1: Overlay of BOLD activation with averaged raw image a) and b) registered to high-resolution reference. c-e) Zoom in on left motor cortex. Veins close to the motor cortex are indicated by white arrows. d) Overlay of registered activation map (FWHM=0); e) Overlay of registered and smoothed map (FWHM=1mm).

uN-BIASED: a nearly model-free fMRI analysis method based on reproducible responses and applied to 7 T clinical fMRI

P. Cardoso, A. Geissler, F. Fischmeister, S. Trattnig, R. Beisteiner, S. Robinson

Purpose/Introduction:
The aim of this study was to develop an analysis method sensitive to activation in regions of pathology, where responses might deviate from predictions due to modified HRF [1]. The suggested method, which we call uN-BIASED, is an extension of the BIASLESS method of Levin et al. (2001) [2] to N runs (N>=2) [3] and is tested on 7T clinical data.

Subjects and Methods:
Ten patients performed 7 to 10 runs of a hand task, which comprised 4 rest and 3 task phases (of 20s each) presented in a block design. EPI data were acquired with a 7T scanner with a 32-channel head coil, with 34 ACPC slices, with a resolution of 1.8x1.8x3 mm and TE/TR=21/2500 ms. Runs were motion corrected and coregistered, and voxels time series were corrected for baseline fluctuations [4].
In the first step of the uN-BIASED method, the beta value for each voxel and each pair of runs was calculated as the fit of the time series for that voxel in run x to that in run y (Fig.1). Subject-level statistics were generated from all non-identical pairs of runs (Fig.2, circled in blue). For each voxel, the number of first level t values above the threshold defined by p<0.001 (uncorr) were counted (Fig.2, “Counts”). Counts (voxel reliability) were used to mask subject-level statistics. Results were compared with the results of a GLM analysis.

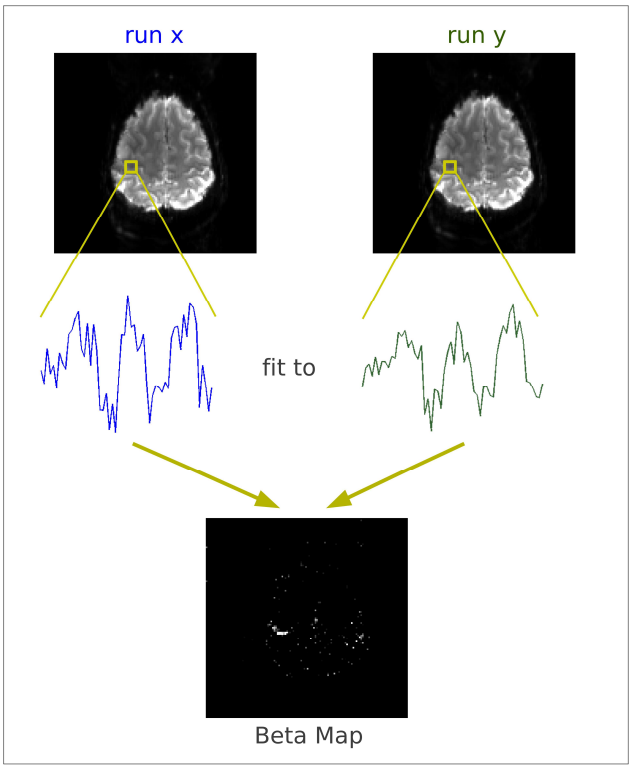

Figure 1. The first step in the uN-BIASED method.

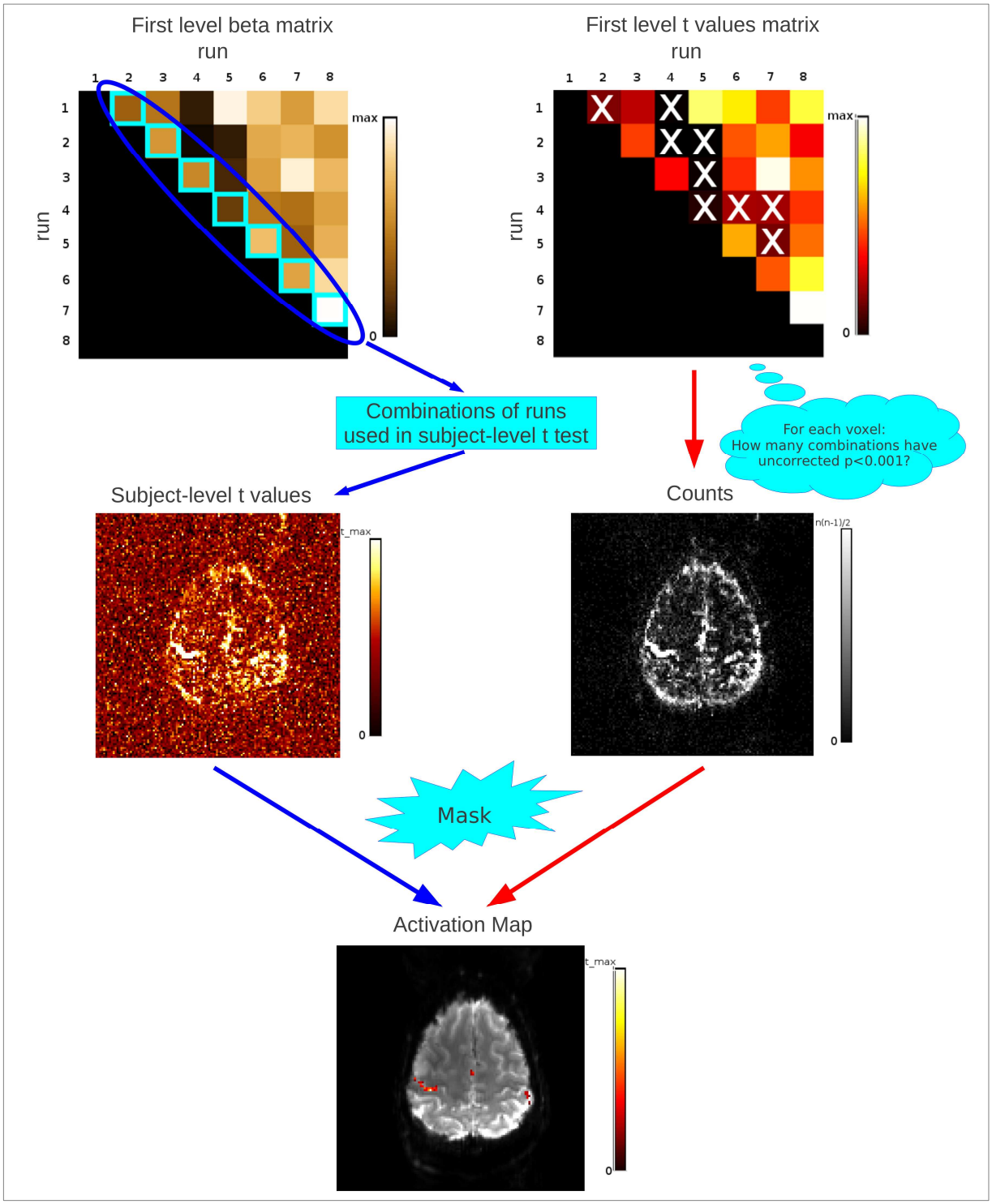

Figure 2. The second stage of the uN-BIASED method illustrated for one subject (P1).

Results:
uN-BIASED results showed activation in known motor regions (Fig.3). There was better separation of activation and artefacts in uN-BIASED than GLM (e.g. P9). Activation was apparent for all patients using a consistency mask in the uN-BIASED approach of n_combs(N), except for P2, for which n_combs(N-1) was appropriate. No activation was apparent in GLM results for P2, P6, P9 and P10 at a FWE corrected threshold of $p<0.05$ (green arrows). At a lower, uncorrected $p<0.001$ threshold, GLM results were noisy compared to uN-BIASED results.

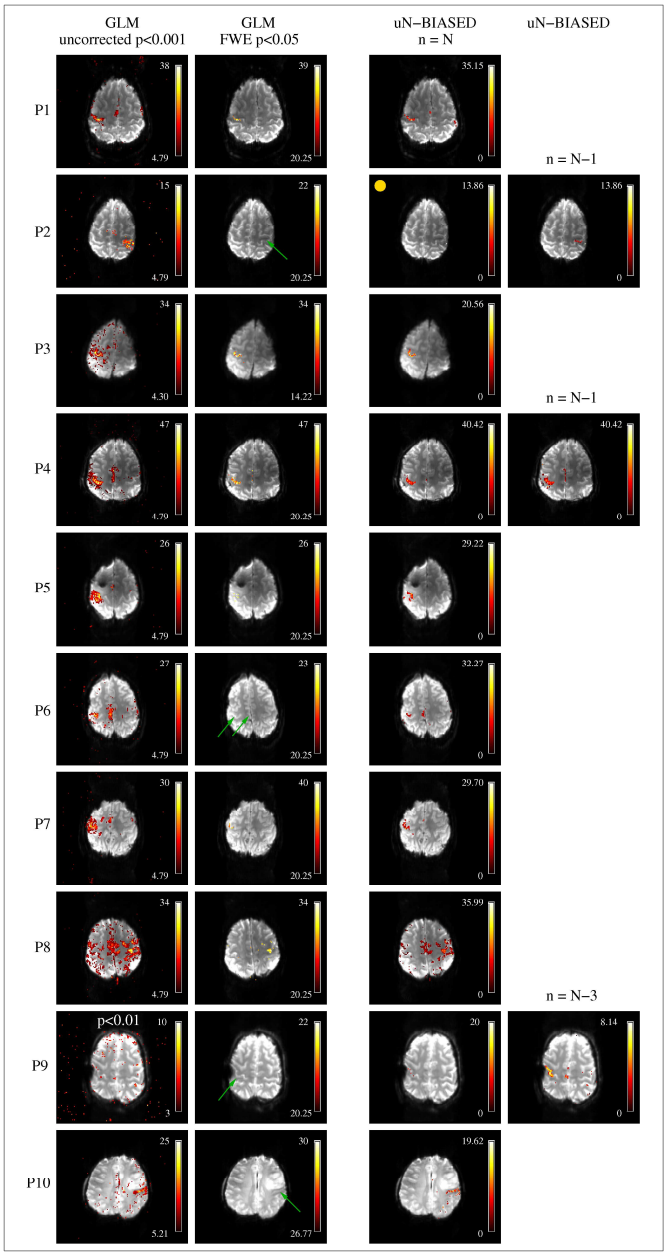

Figure 3. A comparison between results obtained with the GLM and uN-BIASED method for ten patients.

Discussion/Conclusion:
The uN-BIASED method makes no assumption about response timing other than that it is consistent over runs. The extension of the BIASLESS approach to N runs allows t-statistics to be calculated and offers a simple approach to thresholding, based on response reliability. The uN-BIASED is expected to be sensitive to neuronal activity when the response does not agree with the GLM prediction due to compromised performance or modified hemodynamic coupling.

References:
[1] Fujiwara, N., et al., NeuroImage (2004); 21: 1464.
[2] Levin, D., et al., NeuroImage (2001); 13: 153.
[3] Beisteiner, R., et al., Neuroscience Letters (2000); 290: 13.
[4] Beisteiner, R., et al., NeuroImage (2011); 57: 1015.

Stability of intraindividual resting-state measurements

Michael Erb

Biomedical Magnet Resonance, University Hospital Tübingen

In order to evaluate the stability of spatial modes in resting state fMRI, a single subject was measured up to now at 18 time points. Several analysis methods were used to find consistent modes including seed region based functional correlation and independent component analysis (ICA).
Image acquisition was performed on a 3T scanner (Siemens MAGNETOM Trio, a TIM System) using a GE-EPI sequence with 32 slices (thickness 3.5 mm + gap 0.5 mm, Matrix 64x64, FoV 192x192 mm2). Each session consist of 305 volumes measured within about 10 minutes (TR = 2s, TE = 30ms) and a T1w structural dataset (MPRAGE, 1mm3 resolution). Data were preprocessed with SPM8 (slice time correction, realignment, coregistration to the structural volume and normalization to the MNI standard space, resliceing to 3x3x3 mm3 voxel, smoothing with FWHM of 6mm). So we are able to compare the activation pattern with data from other groups. In order to reduce the effect of motion related signals, we subtracted the signal estimated by a GLM with realignment parameter regressors.
The main evaluation was done using group independent component analysis, implemented in MATLAB by Calhoun et al. (Group ICA of fMRI Toolbox, GIFT [1]). Corresponding to the article of Allen et al. [2], we choose the number of components to 28 (low dimensional analysis) and 75 (high dimensional analysis). Each data set was analyzed two times: First in a separate single session model and then together with all other sessions in a full group analysis. The resulting independent components (ICs) were spatial sorted compared to the resting state network (RSN) components described in [2].
Spatial sorting with the group ICs allows identifying the corresponding ICs from single study analyses. For each group IC we calculate the ratio between best and second best match.
Results
After correction with movement parameter, group ICA showed a very stable set of components. In the analysis with 75 ICs we found about 40 of the 75 ICs with 2nd best watch only half or less of the best match (Figure 1). Nevertheless, detailed analysis disclosed a significant dependency on subject states (sleep, hunger, satiety).
Resting stare fMRI has become a very powerful tool to analyze brain connectivity. But even with repeated measurement of the same subject, we found a quite big variability of pattern. Take into account of different subject states allows reducing the unexplained variability.
References
[1] Calhoun V.D., Adali T., Pekar J.J., and Pearlson G.D., Latency (in) Sensitive ICA: Group Independent Component Analysis of FMRI Data in the Temporal Frequency Domain NeuroImage, vol. 20, 2003.
[2] Allen EA, et al., A baseline for the multivariate comparison of resting-state networks. Front Syst Neurosci. 2011 Feb 4;5:2.

Resting state evaluations in a group of MS patients

E. Charyasz, B. Bender, U. Klose

Tübingen, Germany

Multiple sclerosis is a chronic, central nervous system disease. Resting state fMRI is often used to assess impaired functional connectivity in brain. We aimed to use rs-fMRI to identify changes in resting state connectivity to determine the effects of duration of disease on networks (basal–ganglia, sensorimotor, visual, default-mode, attentional, frontal and auditory) in patients with MS. Data was collected on a 3T MR scanner (Trio Tim, Siemens), analysed using SPM8 and a group independent component analysis (ICA). 53 patients with multiple sclerosis were included and divided into 5 groups depending on the duration of the disease. 7 networks were identified in each group. No significant resting state differences were found between groups.

Analysis of resting state signal variations in patients with Friedreich´s ataxia

Maximilian Löffler

The disease of Friedreich's ataxia is clinically described by various neurological symptoms, reaching from decreased functions of motor coordination over impairment of vision and hearing to loss of neuroendocrine function presented by diabetes. Neuropathological examinations showed neural degeneration in white matter tracts as well as gray matter nuclei. Assessing alterations in resting state brain networks therefore could be a general approach to cover these changes. The data of functional magnetic resonance imaging is processed by an independent component analysis (ICA) to reveal such networks and draw inferences about functional connectivity in the brain. However this novel technique poses some challenges when it comes to between group comparison - especially in small groups of only 8 patients and healthy volunteers respectively - since ICA doesn't provide an inherent model about making inferences as in block-design fMRI studies. We currently focused on comparing extent and peak t-value (one-sample t-test) of corresponding clusters of independent components in the two groups. Preliminary results show increased spatial size of clusters representing parts of the sensory-motor network and partially higher peak t- values in the group of patients compared to healthy controls.

Wednesday, June 27, 2012

8:30-10:30 Scientific session 6

A multi-channel $^{1}H/^{31}P$ transmit-receive coil for spectroscopy in the human calf at 7T
S. Goluch, R. Kriegl, E. Moser, T. Herrmann, J. Mallow, J. Bernarding, K.-N. Kim, S.-M. Hong, H.-B. Jeong, Z.-H. Cho, E. Laistler

A coil for very small specimens to be used in a clinical 3T MRI scanner environment. Challenges and solutions.
M. Burian, J. Rydlo, M. Hajek

Inductive Decoupling of Monolithic Transmission Line Resonators
R. Kriegl, J.C. Ginefri, M. Poirier-Quinot, L. Darrasse, E. Moser, E. Laistler

Local investigation of RF induced pacemaker heating in MRI at 1.5T and 3T
G. Fiedler, E. Moser, A.I. Schmid

RF coils for high-field ^{13}C MRS in humans
Martin Meyerspeer

SendMeClever - Web based tool for transfering MR data
Jiru F, Hajek M

A multi-channel $^{1}H/^{31}P$ transmit-receive coil for spectroscopy in the human calf at 7T

S. Goluch[1,2], R. Kriegl [1,2,3], E. Moser[1,2], T. Herrmann□, J. Mallow□, J. Bernarding□, K.-N. Kim[5], S.-M. Hong5, H.-B. Jeong5, Z.-H. Cho5, E. Laistler1,2

[1] MR Center of Excellence, Medical University of Vienna, Vienna, Austria, [2] Center for Medical Physics and Biomedical Engineering, Medical University of Vienna, Vienna, Austria, [3] IR4M (Imagerie par Résonance Magnétique Médicale et Multi-Modalités), UMR8081 CNRS, Université Paris Sud 11, Orsay, France, □ Department of Biometry and Medicine Informatics, OvG University Magdeburg, Magdeburg, Germany □ Neuroscience Research Institute, Gachon University of Medicine and Science, Incheon, South Korea

Introduction

^{31}P spectroscopy is employed for studying energy metabolism in the muscle. At 7T, this technique benefits from higher sensitivity and increased spectral resolution, as well as shorter relaxation times[1]. The purpose of this work is to design a sensitivity-optimized double-tuned $^{1}H/^{31}P$ transmit-receive surface coil fitting the human calf for muscle metabolism studies at 7T.

Methods

The coil (Fig.1) consists of two proton channels (12.5x12.5cm²) with shared conductor and a three channel overlapped ^{31}P array (element size 10x7cm²). The structure was bent into cylindrical shape with diameter of 16.9cm(^{1}H) and 14.9cm(^{31}P). Segmenting capacitors were evenly distributed over the wire length at distances<λ/20. Proton channels were decoupled with a capacitor on the shared conductor, adjacent phosphorus channels were overlapped. The coil was loaded with a cylindrical phantom (d=13.3cm) filled with a gel consisting of 30mmol/l ^{31}P in K_2HPO_4, 1ml/l Magnevist, 1.25g/l NaCl, and 10g/l polyacrylic acid. With a conductivity of 0.77 S/m and a physiological ^{31}P concentration[2] it should act as a realistic model of the calf muscle. To achieve best B_1□ efficiency and homogeneity, 3D EM simulation using XFdtd and Matlab was used to determine the optimal phase relation between channels. Due to homogeneity of the phantom, spatial distribution of the ^{31}P signal amplitude can serve as a measure for relative B_1□ distribution. Therefore, a metabolic map (fitted area under peak) was acquired with a 2D CSI sequence on a Siemens 7T whole-body system.

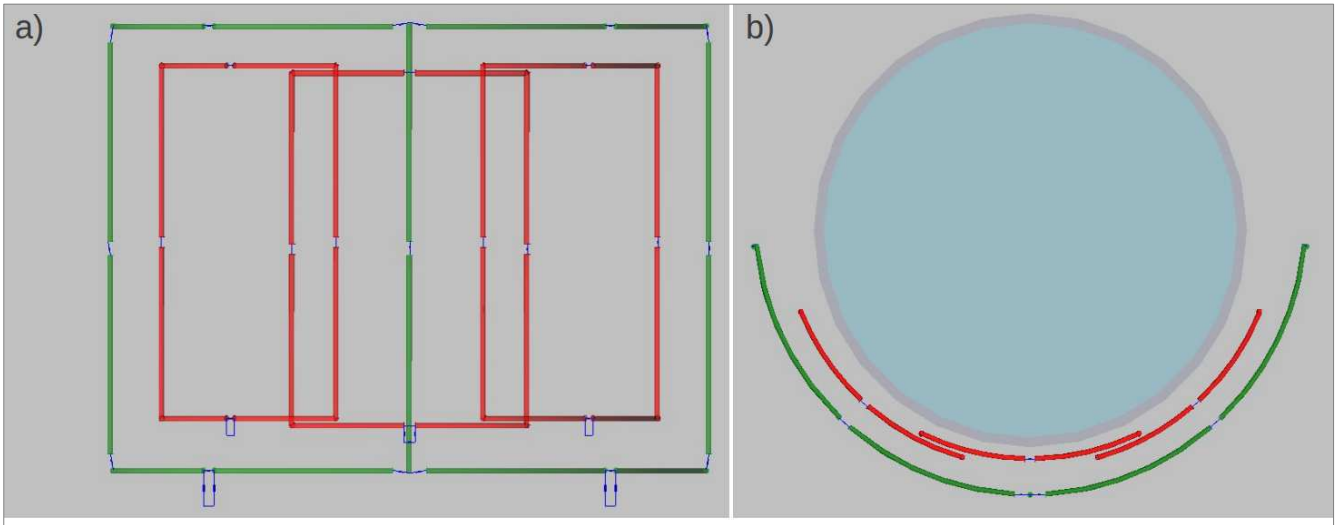

***Fig. 1** XFdtd 7.2.2 (Remcom,State College,PA,USA) model of the ^{1}H (green)/^{31}P (red) coil in **(a)** front, **(b)** bottom with phantom (blue) view.*

Results

Decoupling of -27dB was achieved for the proton coils, decoupling between ^{31}P channels was <-12dB. Cross-coupling between ^{1}H and ^{31}P channels was <-14dB@120.3MHz and <-21dB@297MHz. Simulation showed optimal B_1^+ distribution for the proton coil in CP mode and phase shifts of 0°/60°/120° for the phosphorous array. The metabolic map is overlaid on a GRE proton image of the gel filled cylinder in Fig.2a. Comparison with the simulation result (Fig.2b) for the combined ^{31}P B_1^+ field shows good agreement.

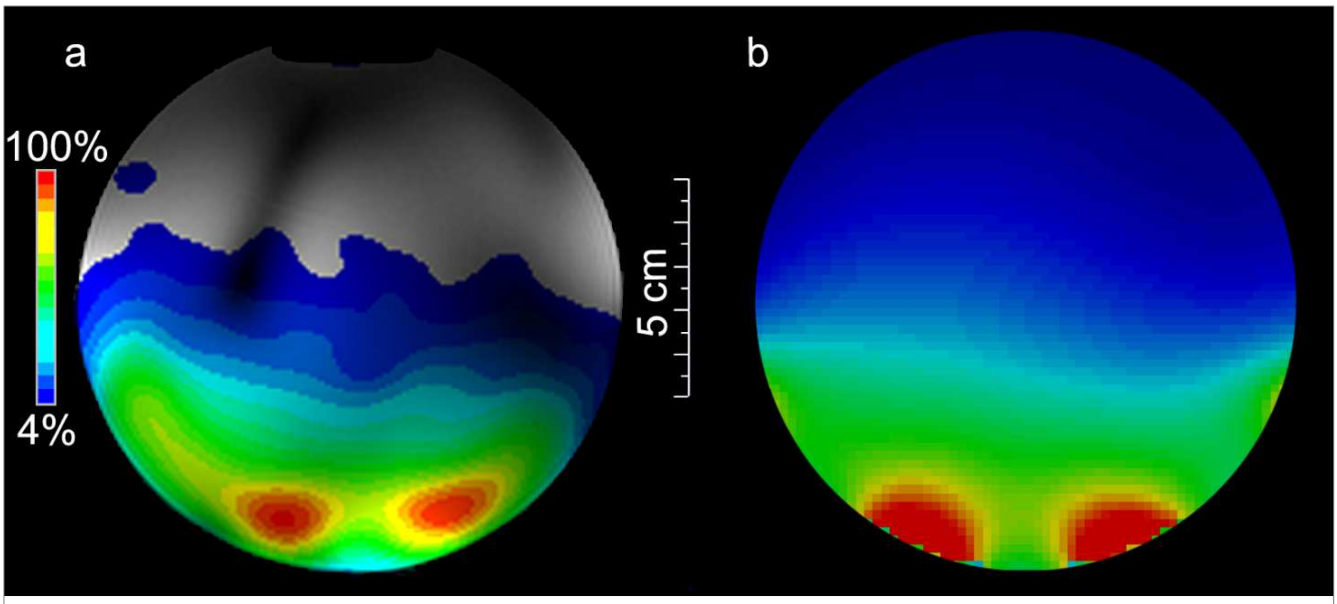

Fig. 2 ***(a)*** *Metabolic map from 2D CSI (sequence parameters: TR=400ms, TE=1ms, FOV=14x14x4cm³, MA=14x14, reconstructed to 32x32), post-processing was performed using the manufacturer's spectroscopy software.* ***(b)*** *Simulated combined B_1^+ field.*

Note that lower signal intensity at the border area of the CSI measurement data is due to partial volume effects.

Discussion/Conclusion

We constructed a highly sensitive ^{31}P array coil with optimized phase combination for 7T. First results are in good agreement with 3D EM simulation. The obtained ^{31}P sensitivity pattern is well-suited for studies examining the gastrocnemius[3]. In a next step, second-order traps will be inserted to minimize cross-coupling between proton and phosphorous coils. Further improvement should be achieved by phase-corrected combination of the individual ^{31}P-signals.

References

[1] Bogner et al, MRM (2009), 62(3):574-82
[2] Kemp et al, NMR Biomed (2007), 20:555-65
[3] Meyerspeer et al, MRM (2012), doi:10.1002/mrm.24205

A coil for very small specimens to be used in a clinical 3T MRI scanner environment. Challenges and solutions.

M. Burian, J. Rydlo, M. Hajek

Purpose / Introduction

A special coil has to be used in order to facilitate measurements of small volume samples such as tissue extracts in small test tubes on a clinical class 3T scanner. While the coil directly improves SNR, new problems can occur. The most prominent one is a failure of adjustment routines. This is caused mainly by the size of the sample and simple methods exist to overcome this limitation.

Subjects and Methods

The coil was built for 3T scanner Siemens Tim Trio. A T/R coil configuration was chosen. It is a single loop made of 25 mm wide adhesive copper tape wound on the PVC-U tube 32 mm in diameter forming a paralel resonant circuit with appropriate chip and trimmer capacitors.

Coil is connected to the scanner through a simple custom made T/R switch based on a classical quarter-wave design. It is assembled of 2 PIN diodes and one quarter-wave coaxial cable section.

The PIN diodes are driven from the scanner by 2 independent control lines. To boost aquired signal, coil was also equipped with low noise preamplifier featuring 26 dB gain and NF <1dB based on single SPF-5189 MMIC (RF Micro Devices). In order to assess an optimal transmitter reference voltage for the coil, A series of one-pulse FID measurements was obtained with reference voltage setting varied manually in order to assess an optimal transmitter reference voltage for the coil. Due to a failure of automated adjustment routine (owing to low voltage required), 10 dB attenuator had to be inserted into transmit path prior to T/R switch. The reference voltage specification in the coil file was appropriately then corrected by 10 dB.

Results

90 degrees pulse reference voltage for the coil corresponds to value of approx. 2.5V. Setting this value to coil file leads a failure of adjustment automations. Implementing the transmit attenuator and correcting reference voltage specification in the coil file to value of 8V made the automations work properly and set the proper pulse voltages to run the experiment.

Discussion/Conclusion

Implementing the attenuator into transmit path we were able to run experiments on small samples without need for manual adjustment of pulses, frequency, etc. This facilitates much the measurement and lowers requirements for machine time.

Acknowledgements:

Supported by: GACR P301/11/2048, ENCITE 7th Framework Program EU (No.: 201842) and

Institutional project 00023001 IKEM by MZCR

References

[1] Lowe IJ, Tarr CE. J Sci Instrum. 1968 Mar;1(3):320-2.

Inductive Decoupling of Monolithic Transmission Line Resonators

Kriegl R.[1,2,3], Ginefri J.C.[1], Poirier-Quinot M.[1], Darrasse L.[1], Moser E.[2,3], Laistler E.[2,3]

[1]IR4M, Université Paris Sud 11, Orsay, France
[2]MR Centre of Excellence, Medical University of Vienna, Vienna, Austria
[3]Center for Medical Physics and Biomedical Engineering, Medical University of Vienna, Vienna, Austria

Introduction: Arrays combine the high signal-to-noise ratio of small surface coils with the extended field of view (FOV) of a single larger coil, provided that the individual elements are sufficiently decoupled. Conventional decoupling techniques use either geometric overlap [1], with the drawback of reduced FOV and higher g-factors for parallel imaging, or LC-networks between non-overlapping coils, with the drawback of frequency and load dependent decoupling efficiency. Further, these techniques are not well suited for double-sided monolithic structures. The goal of our work is to construct an array of inductively decoupled monolithic transmission line resonators (TLR) [2]. TLRs consist of two conducting loops deposited on both sides of a low-loss dielectric substrate providing an integrated, distributed capacitive effect minimizing stray E-fields in the sample. TLRs can be fabricated with high reproducibility and are flexible in shape due to the low substrate thickness (0.1–1mm) [3].

Methods: To decouple the elements within an array of TLRs, the basic geometry (Fig.1) was extended by small annexes. Neighboring elements are decoupled by overlapping a front-sided annex of one element with a back-sided annex of the other element. Four annexes per element permit decoupling from next neighbors in 2D-arrays.

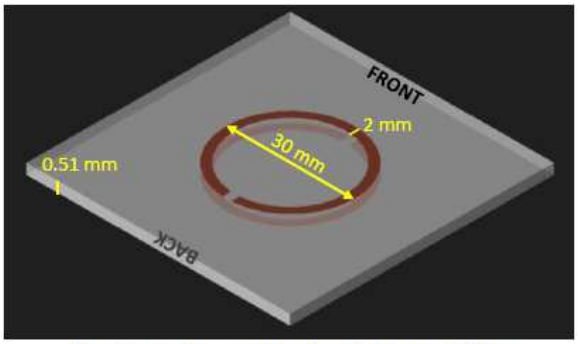

Fig. 1: Schematic depiction of the monolithic transmission line resonator

To test this technique, a two-element array (2mm spacing between coils) designed to resonate at 297.2 MHz (i.e. ^{1}H at 7T) was etched from CuFlon® microwave substrate. Standard capacitive matching was implemented, S-parameters and Q-factors were measured. GRE images (Siemens 7T whole-body scanner) of a cylindrical phantom (r=6cm, h=20cm) were acquired in receive-only mode. A separate birdcage coil (RAPID Biomedical, Rimpar, Germany) was used for transmission, receive elements were passively detuned using crossed PIN diodes.

Results: The elements of the fabricated array were matched (<-40dB) and efficiently decoupled (<-21dB) with our technique (Fig.2). The mean individual quality factors of the coils are 135 in unloaded condition and 33 when loaded by the phantom. A phantom image is shown in Fig.3.

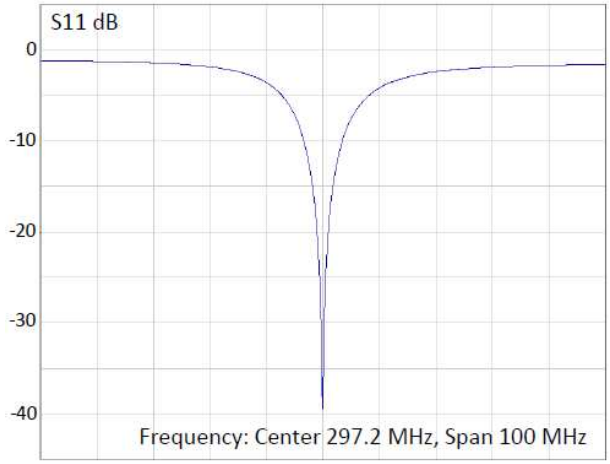

Fig. 2: S11 parameter in the loaded condition; No splitting caused by coupling to the other element can be observed

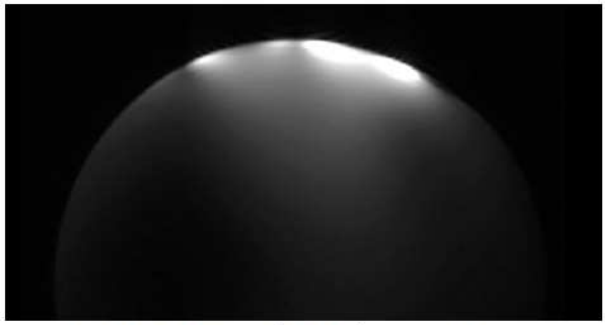

Fig. 3: Transversal GRE phantom image, 0.67x0.67x3 mm resolution

Discussion:

The presented decoupling technique is frequency and load independent over a wide range, similar to conventional overlap decoupling, while retaining the FOV of non-overlapped coils, and presumably improving parallel imaging performance. Here, our technique is demonstrated on a two-element structure; however, it can be easily expanded to multi-element linear or 2D-arrays and, in principle, also to non-monolithic designs. Our approach will enable the production of readily decoupled arrays with arbitrary number of elements in a single etching process.

References:

[1] Roemer,P.B.,1990,MRM,192-225.
[2] Serfaty,S.,1997,MRM,687-689.
[3] Woytasik,M.,2007,Microsyst Technol,1575-1580.

Local investigation of RF induced pacemaker heating in MRI at 1.5T and 3T

G. Fiedler, E. Moser, A.I. Schmid

Medizinische Universität Wien

Purpose / Introduction RF pulses are known to induce heating in pacemaker leads, in particular at their tips, wherelocal tissue burning can block the pacemaker's function.

Subjects and Methods A pacemaker (leadlength=58.8cm) was placed in a phantom of 28l polyacrylic acid gel (65x42x9cm) following ASTM F2182-11a. Local temperature was measured during MRI scans using fluoroptic thermosensors (Neoptix Inc.). One sensor was placed contacting the tip (Fig.1B), another one was placed in various positions, including the wire, the pacemaker housing or other places in the gel. A wide range of geometries, positions and imaging sequences were investigated, in both 1.5T and 3T scanners. The built-in body coil was used for imaging. Heating is expressed as $\Delta T/\Delta t$ during the first 10s of each scan.

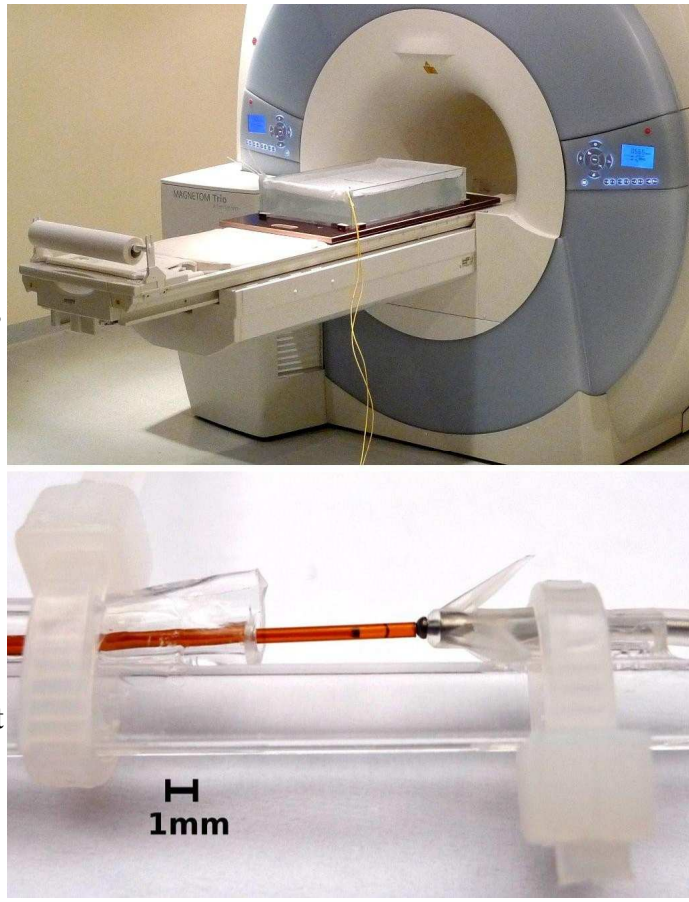

Figure 1: A) Gel setup B) fluoroptic thermosensor (left) at tip of pacemaker (right).

Results Placing all the lead and the pacemaker central (regarding the phantom) consistently resulted in low heating. Keeping the pacemaker and the tip in place but moving the majority of the lead parallel to B0 and closer to the phantoms left wall resulted in increased heating of the tip, being significant when closer than 8cm to the wall (Fig.2A/3A). Increasing the length of the segment running close to the wall further increased heating (Fig.2B/3B).

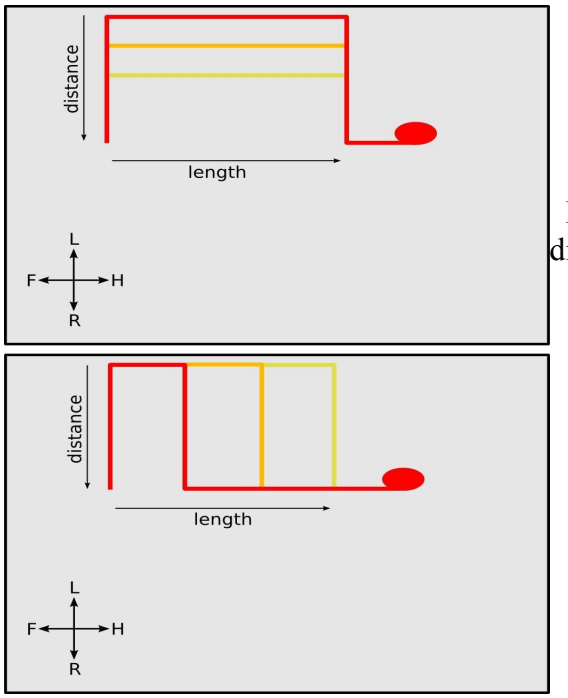

Figure 2: Geometries of lead in phantom for A) distance and B) length measurements.

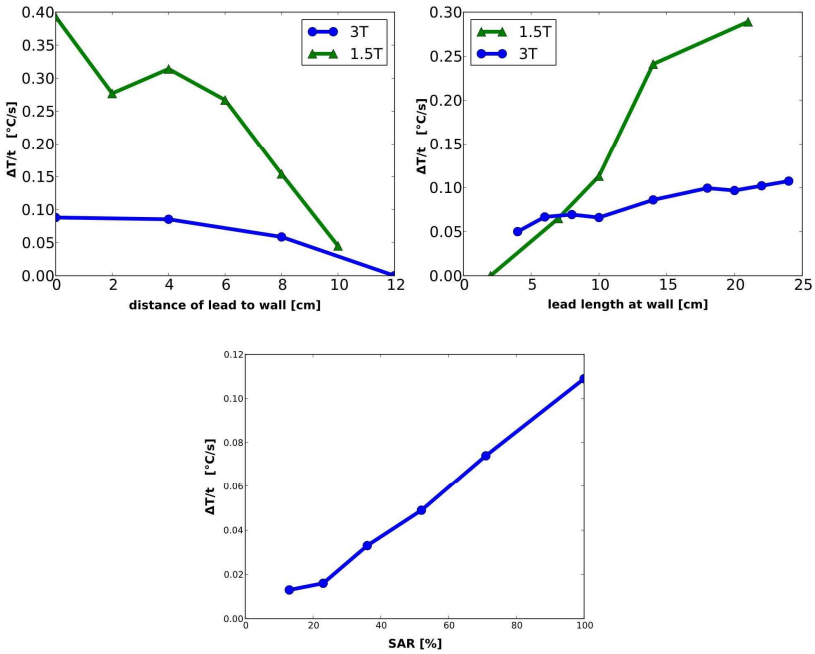

Figure 3: Correlation of heating with A) distance to the wall (length=24cm), B) length at the wall (distance=1cm) and C) shown SAR value (distance=1cm, length=24cm). Within the same setup we found that heating rises approximately linear with the SAR value reported by the scanner (Fig.3C).

We also measured significant heating with the lead in a central position (regarding left-right), but on the surface of the gel. The lead orientated in left-right direction also resulted in significant heating, although less than in head-foot orientation. No difference was obtained regarding the type of sequence (gradient echo, turbo spin echo). Strong gradients without SAR emerged no heating (epi with RF=0).

Discussion/Conclusion Heating was significantly stronger at 1.5T compared to 3T, probably depending on lead length [1]. Heating depends strongly on the length of the superficially running part of the lead and SAR. Current pacemaker designs cannot be regarded safe for MRI when using the body coil for excitation, regardless of image position.

References [1] Nordbeck, P., 2012, Magn.Reson.Med. doi:10.1002/mrm.24197
Supported by: FFG, RSA

Sensitivity analysis of mutli-nuclear coils with proton traps

M. Meyerspeer[1,2], E. Serés Roig[2], E. Moser[1], R. Gruetter[2, 3], A.W. Magill[2]

[1] Vienna Medical University, Vienna, Austria
[2] École Polytechnique Fédérale de Lausanne, Switzerland,
[3] Université de Genève, Switzerland

Purpose / Introduction Proton traps have been used for the last few years to suppress coupling of ^{1}H coils to non-proton coils in multi-nuclear coil arrangements with separate channels [1,2]. The original design, consisting of an inductor and a capacitor in parallel (a first-order element) has been modified by Webb et al. [3] adding a series capacitance, which makes it possible to put the trap in place of a coil capacitor.

We have previously given an analysis of these second-order traps' design criteria and properties and reported experimentally-found advantages on coil SNR [4]. However, analytic and quantitative analysis of this SNR benefit have not been not explored in full detail and under different loading conditions.

Subjects and Methods The impact of first-and second-order traps on coil sensitivity was modelled by taking into account resistive losses introduced by the traps.
Rather than assuming Q or R to be independent of L, previously shown to yield higher SNR with second-order traps, resistive losses were estimated via the traps' Q-factor, employing $R = \omega L / Q(\omega,L)$. The traps' quality-factor was measured for a range of choke-inductances L, after tuning the traps to the X-nuclear MR-frequency (^{13}C(7T): 75 MHz) by exchanging its capacitors for bigger values (to operate as current block at ^{1}H frequency, traps are tuned to 297 MHz).

Results Linear regressions of $R(L)$ (Fig. 1) were used in the model of trapped-coil SNRs and compared to experimentally measured sensitivities under different loads (Figs. 2,3).

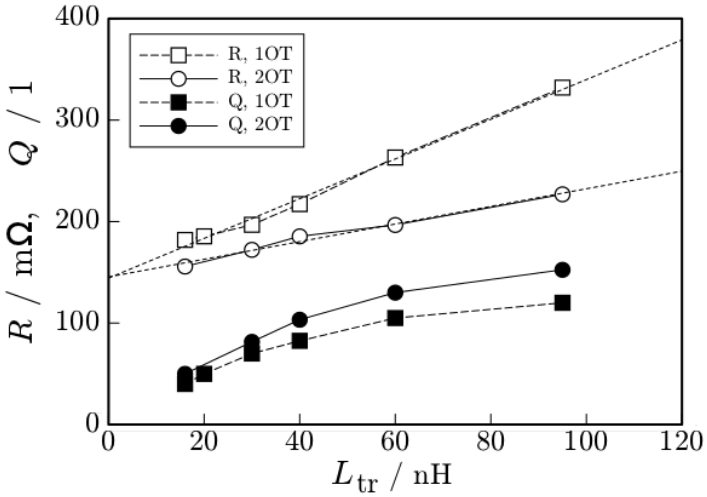

Fig. 1: Q-factors and corresponding series resistances R of isolated traps at 75 MHz.

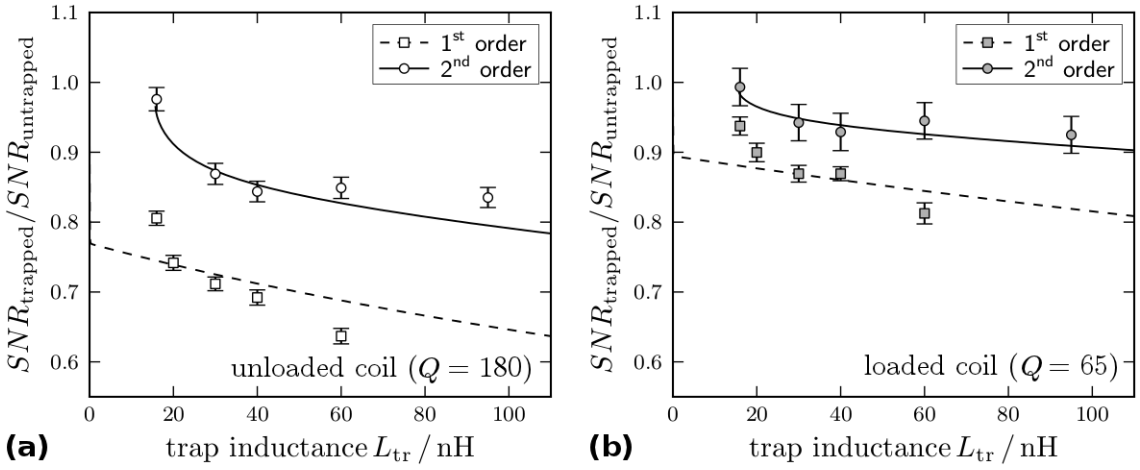

Fig. 2: Simulated (lines) and measured (mean ± SD) relative sensitivity of trapped vs. untrapped ^{13}C coils (a) unloaded and (b) loaded.

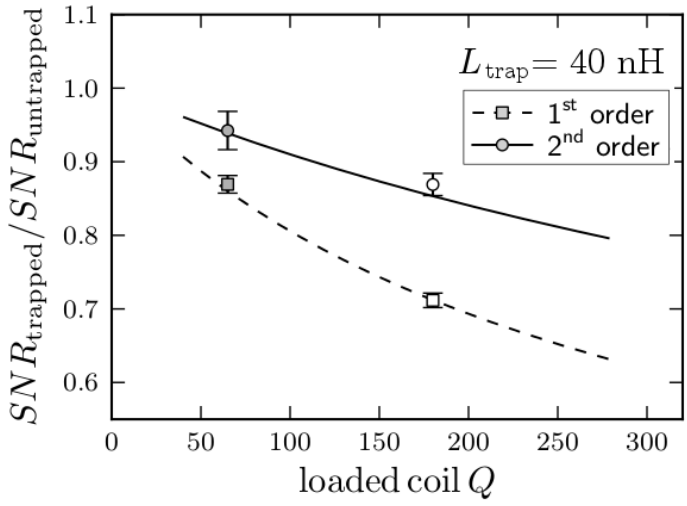

Fig. 3: Simulated relative sensitivity of trapped coils (L = 40 nH) under varying load and coil sensitivities measured using a sniffer loop (mean ± SD).

Coil sensitivities (SNR) were verified in ^{13}C-NMR experiments, showing consistent results.

Discussion/Conclusion Although for loaded coils sample-noise dominates, the sensitivity-loss introduced by a coil trap is not negligible and was shown to be on the order of 10 % for first-order traps and ca. 5 % when using second-order traps. The benefit is more pronounced under sub-optimal loading conditions (10 % vs. 30 %), as forcibly is the case e.g. for some elements in array-coils, where second-order traps can contribute considerably to achieve highly efficient multi-nuclear coil designs.

References

[1] Alecci et al. JMR:181(2006)
[2] Dabirzadeh, McDougall. Concepts-in-MR-B:35(2009)
[3] Webb and Smith. ISMRM(2010)/Stockholm #3818
[4] Meyerspeer et al. ESMRMB(2011)/Leipzig #240

Acknowledgements: FWF/J3031-N20. FFG/832107. CIBM/EPFL and Leenaards and Jeantet Foundations

SendMeClever - Web based tool for transfering MR data

Jiru F, Hajek M

IKEM Prague

Introduction: Research cooperation between different MR sites often requires sharing of MR data and MR related computing resources. For transferring MR data with sensitive personal information use of secured data transfer protocols (such as SSL/https or sFTP) or data anonymization are mandatory. Difficult access to tools providing these services may lead to using alternative data exchange services (such as FTP or email) that compromise data security. In this contribution SendMeClever application for MR data exchange conforming to above mentioned security requirements is introduced.

Program description: SendMeClever is a web application running in conventional web browser that enables:

1) Sending email like messages with large attachments over secured https connection. This simplifies data description in the message because cryptic names for personal data in MR data headers are not required. The whole directory structure containing e.g. selected MR study can be selected as an attachment.

2) Processing MR data in the attachment prior to the delivery to the recipient using extendable processing utilities. SendMeClever currently implements DICOM anonymization which obviates separate data anonymization before sending.

3) Sending attachment data to Java Message Service (JMS) provider for asynchronous data processing. This feature enables automatic processing of attachment data by the program installed at the recipient's site.

Grant sponsors:
Supported by the Ministry of Health, Czech Republic (grant 00023001 IKEM).

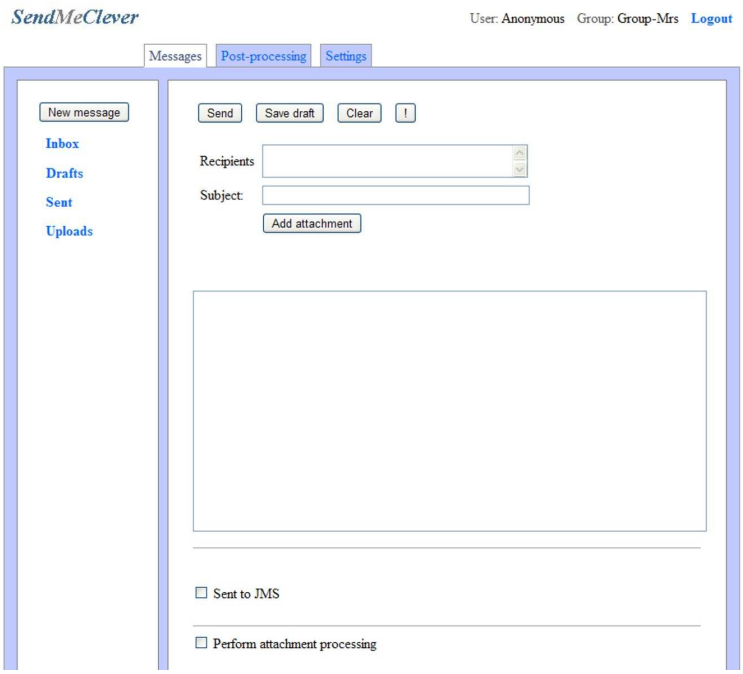

Fig.1 Snapshot of the SendMeClever website

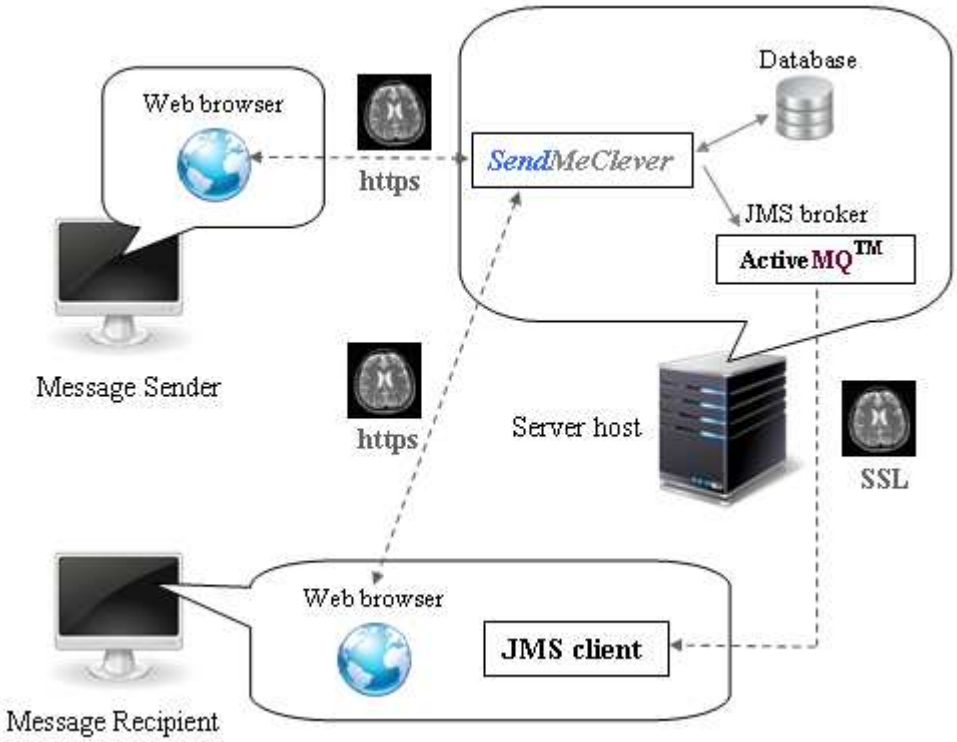

Wednesday, June 27, 2012

11:00-13:00 Scientific session 7

The impact of baseline variations in quantitative analysis of in-vivo spectra
A. Gröger

Progressive ataxia with an unknown signal in ^{1}H MR brain spectra
M. Dezortova, K. Brozova, M. Hajek

Quantitative MR imaging and spectroscopy of brain tumours
D. Wagnerova, V. Herynek, A. Malucelli, M. Dezortova, J. Vymazal, D. Urgosik, M. Syrucek, F. Jiru, A. Skoch, R. Bartos, M. Sames, M. Hajek

Iron deposition in the basal ganglia in patients with a brain tumor
V. Herynek, D. Wagnerová, A. Malucelli, J. Vymazal, M. Hájek

3D ASL at 7 Tesla: Initial Results
K. Schewzow

The impact of baseline variations in quantitative analysis of in-vivo spectra
A. Gröger

Progressive ataxia with an unknown signal in 1H MR brain spectra

[1]Monika Dezortova, [2]Klara Brozova, [1]Milan Hajek

[1)] MR-Unit, Department of Diagnostic and Interventional Radiology, Institute for Clinical and Experimental Medicine, Prague, Czech Republic
[2)] Department of Child Neurology, Thomayer Hospital, Prague, Czech Republic

We report a case that represents, to our knowledge, an unknown disease characterized by a new, as yet undescribed signal in 1H MR spectra of the brain.
Female patient with progressive ataxia and spasticity since infancy, without neurological problems in the family, was repeatedly examined using MRI and MRS.
The first MRI at the age of 2 years indicated leukodystrophy. Another MR examination including MRS was performed when she was 14, 16 and 18 years old. MRI revealed supratentorial dystrophic changes predominantly affecting the white matter, with progressive atrophy.
PRESS sequence in the frontoparietal white matter with TR/TE=5000/30, 80, 135 and 270 ms was used for MR spectroscopy and revealed low NAA and choline and high myo-inositol. In addition, a new signal visible at 2.13±0.01 ppm was repeatedly detected even in spectra with a long TE.
The new signal was assigned to a methyl or even an acetyl group of a small and relatively mobile molecule or as a simple radical of a larger rigid molecule. From the potential candidates, we highlighted methionine as the key compound.
So far, we have not better hypothesis. Maybe there are some unpublished MR spectra or other clinical data that could support our results.

The study was supported by the MZCR institutional project 00023001IKEM.

Quantitative MR imaging and spectroscopy of brain tumours

Dita Wagnerova[1], Vit Herynek[1], Alberto Malucelli[2], Monika Dezortova[1], Josef Vymazal[3], Dusan Urgosik[4], Martin Syrucek[5], Filip Jiru[1], Antonin Skoch[1], Robert Bartos[2], Martin Sames[2], Milan Hajek[1]

[1] Department of Diagnostic and Interventional Radiology, Institute for Clinical and Experimental Medicine, Prague, Czech Republic
[2] Department of Neurosurgery, JE Purkyne University and Masaryk Hospital, Usti nad Labem, Czech Republic
[3] Department of Radiology, Na Homolce Hospital, Prague, Czech Republic
[4] Stereotactic and radiation neurosurgery, Na Homolce Hospital, Prague, Czech Republic,
[5] Department of Pathology, Na Homolce Hospital, Prague, Czech Republic

Coregistration of different MR images and their subsequent correlations based on pixel-by-pixel quantitative analysis have a potential to distinguish pathological states and a healthy tissue and therefore help assess the brain tumour extent. Patients with low and high grade gliomas, lymphomas, recurrent tumours or radiation necrosis were involved in the study to validate the use of this method in clinical practice.
Two groups of patients with a suspected intracranial tumour and 55 healthy subjects were examined on a 3T system (untreated brain lesions, lesions treated by chemo/radiotherapy). The measurement protocol consisted of MRI, spectroscopic imaging, DTI and T2 relaxometry.
Specific correlation patterns between metabolic concentrations and mean diffusivity (MD) or T2 relaxation times (T2) were found for given lesion localization and for given tumour type. Recurrent tumours exhibited the same correlation patterns as untreated ones, but different parameter values were found in the surrounding irradiated tissue. Metabolic values did not correlate with MD and T2 in the case of radiation necrosis.
A quantitative analysis of different MR methods is able to describe the complexity of a highly heterogeneous tissue in the tumour and its vicinity and determines crucial parameters for tissue differentiation and for assessment of the tumour extension. However this method can be used only in semiautomatic mode due to an unavoidable chemical shift artifact in SI and image distortions in DTI.
Supported by MZCR projects IGA NS/9654-4 and Institutional grant 00023001IKEM.

Iron deposition in the basal ganglia in patients with a brain tumor

Vít Herynek, Dita Wagnerová, Alberto Malucelli, Josef Vymazal, Milan Hájek

IKEM, Prague

Purpose/Introduction

Alterations in iron metabolism accompany a row of diseases. Increased iron concentration is associated also with an increased risk of cancer. We retrospectively evaluated abnormal iron accumulation in the basal ganglia (BG) in patients with a brain tumor using T2 relaxometry.

Subjects and Methods

We examined 23 patients (mean age 48±13 years) with a newly diagnosed brain tumor (14 subjects) or with a tumor recurrence after resection (9 subjects) together with a group of 19 age-matched healthy controls. A standard imaging protocol on a 3T clinical MR scanner was supplemented by a CPMG sequence (32 echoes, TE=13.2 ms, TR=3000 ms, slice through BG). T2 maps were calculated using a three-parameter fit in the globus pallidus (GP),

putamen (Put), caudate nucleus (CN), thalamus (Th), white matter (WM). T2 values were processed contralaterally to avoid a possible edema accompanying the tumor.
The subjects provided an informed consent, used protocols are certificated according to the ISO 9001:2008 norm.

Results

We found significantly lower T2 relaxation times in GP, Put, CN, and Th ($P<0.05$) in patients compared to controls. Patients with a newly diagnosed brain tumor had T2 decreased in GP, CN, Th; patients with a recurrent tumor revealed significantly lower T2 values in GP, Put, CN, and Th. No statistically significant difference was found between patients with a newly diagnosed and recurrent brain tumor. No T2 change was observed in the white matter.

Discussion

The T2 decrease in BG is apparently caused by paramagnetic ion accumulation, probably iron, whose metabolism is known to be altered in relation to a tumor. We speculate that altered iron equilibrium represents an increased risk of an oxidation stress. Surplus iron is therefore oxidized and stored as ferritin. This accelerated protective process may lead to increased iron deposition in BG or Th. Direct damage to BG by the active tumor is improbable (alterations are observed contralaterally) and no damage to the blood brain barrier was confirmed (no signal enhancement in contrast enhanced images in BG). Moreover, no change was found in the white matter, where most of the tumors were located.

Conclusion

The study demonstrates changes in T2 in the basal ganglia of patients with a brain tumor corresponding to increased deposition of paramagnetic ions. These changes occurred in the case of both untreated and recurrent tumors regardless of their localization.

Grant support:IGA MZCR NS/10523-3, Institutional grant 00023001IKEM.

3D ASL at 7 Tesla: Initial Results

K. Schewzow, E. Moser, A.I. Schmid

Medizinische Universität Wien

Arterial spin labeling (ASL) represents a truly non-invasive assessment of tissue perfusion. The potential benefits of this technique at 7 Tesla are the increased perfusion weighted (PW) signal due to higher SNR and the prolonged T1-relaxation times at higher field strengths, allowing for longer inflow and imaging times. There are, however, also challenges in ASL at ultra high field, arising from B0/B1 inhomogeneities, shorter T2/T2* times and SAR constrains. The goal of this work is to implement and optimize the 3D-GRASE based ASL technique for 7T with respect to image quality and SAR.

Supported by
„Aktion Austria - Czech Republic“
63p18